HHS Public Access

Author manuscript

Structure. Author manuscript; available in PMC 2020 November 05.

Published in final edited form as:

Structure. 2019 November 05; 27(11): 1660–1674.e5. doi:10.1016/j.str.2019.08.010.

Convergent evolution of the barnase/EndoU/colicin/RelE (BECR) fold in antibacterial tRNase toxins

Grant C. Gucinski[1,‡], **Karolina Michalska**[2,3,‡], **Fernando Garza-Sánchez**[4], **William H. Eschenfeldt**[2], **Lucy Stols**[2], **Josephine Y. Nguyen**[4], **Celia W. Goulding**[5,6], **Andrzej Joachimiak**[2,3,7], **Christopher S. Hayes**[1,4,*]

[1]Biomolecular Science and Engineering Program, University of California, Santa Barbara, USA

[2]Midwest Center for Structural Genomics, Argonne National Laboratory, USA

[3]Structural Biology Center, X-ray Science Division, Argonne National Laboratory, USA

[4]Department of Molecular, Cellular and Developmental Biology, University of California, Santa Barbara, USA

[5]Department of Molecular Biology & Biochemistry, University of California, Irvine, USA

[6]Pharmaceutical Sciences, University of California, Irvine, USA

[7]Department of Biochemistry and Molecular Biology, University of Chicago, USA

Summary

Contact-dependent growth inhibition (CDI) is a form of interbacterial competition mediated by CdiB-CdiA two-partner secretion systems. CdiA effector proteins carry polymorphic C-terminal toxin domains (CdiA-CT), which are neutralized by specific CdiI immunity proteins to prevent self-inhibition. Here, we present the crystal structures of CdiA-CT•CdiI complexes from *Klebsiella pneumoniae* 342 and *Escherichia coli* 3006. The toxins adopt related folds that resemble the ribonuclease domain of colicin D, and both are isoacceptor specific tRNases that cleave the acceptor stem of deacylated $tRNA_{GAU}^{Ile}$. Though the toxins are similar in structure and substrate specificity, $CdiA\text{-}CT^{Kp342}$ activity requires translation factors EF-Tu and EF-Ts, whereas $CdiA\text{-}CT^{EC3006}$ is intrinsically active. Further, the corresponding immunity proteins are unrelated in sequence and structure. $CdiI^{Kp342}$ forms a dimeric β-sandwich, whereas $CdiI^{EC3006}$ is an α-solenoid monomer. Given that toxin-immunity genes co-evolve as linked pairs, these observations suggest that the similarities in toxin structure and activity reflect functional convergence.

*Lead Contact, Ph: (805) 893-2028, chayes@lifesci.ucsb.edu.

Author Contributions

Conceptualization, K.M. and C.S.H.; Methodology, G.C.G, K.M. F.G.S., W.H.E. and L.S..; Validation, W.H.E., J.Y.N. and L.S.; Investigation, G.C.G., K.M. and F.G.S.; Writing – Original Draft, K.M. and C.S.H.; Writing – Review & Editing, K.M., C.W.G., A.J. and C.S.H.; Visualization, K.M. and C.S.H.; Funding Acquisition, C.W.G., A.J. and C.S.H.; Supervision, A.J. and C.S.H.

‡These authors contributed equally

Declaration of Interests

The authors declare no competing interests.

Graphical Abstract

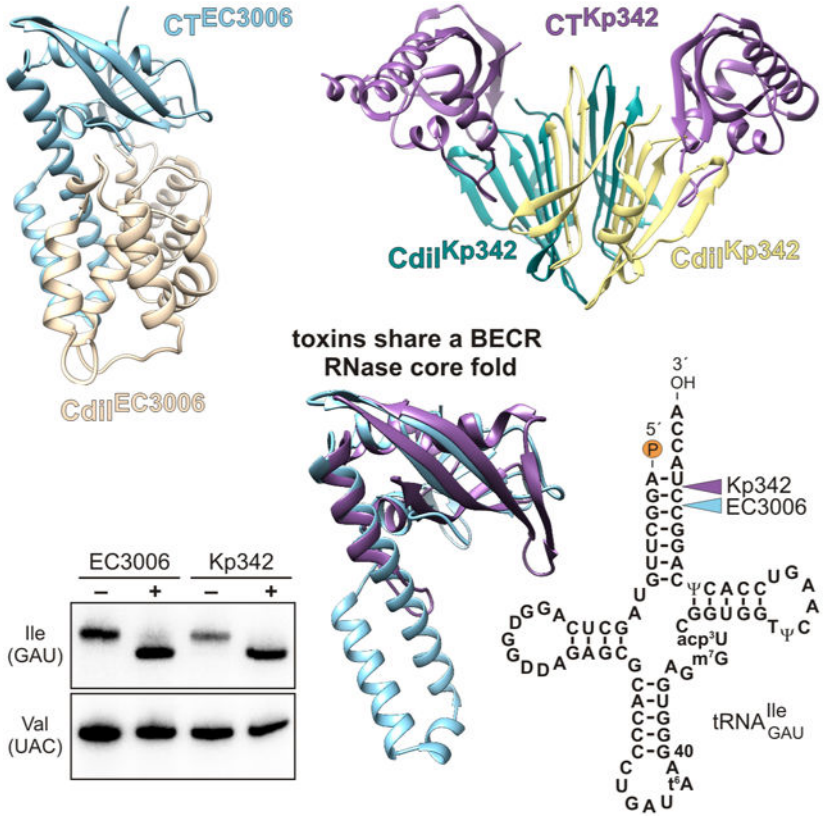

eTOC

Gucinski *et al.* present the structures of two CdiA toxin domains in complex with their cognate immunity proteins. These toxins adopt the same fold and exhibit similar tRNase activities. The immunity proteins are completely unrelated in sequence and structure, suggesting that similarities shared by the toxins arose through convergent evolution.

Keywords

bacterial competition; toxin-antitoxin systems; two-partner secretion; type V secretion system

Introduction

Contact-dependent toxin delivery has emerged as an important general mechanism by which bacteria compete with neighboring cells. Gram-negative bacteria use type I (Garcia-Bayona et al., 2017), type IV (Souza et al., 2015), type V (Aoki et al., 2005) and type VI (Hood et al., 2010; MacIntyre et al., 2010) secretion systems to transfer toxic effector proteins directly into target cells. Similarly, Gram-positive species use the general secretory pathway and type VII secretion systems to compete with neighboring bacteria (Cao et al., 2016; Koskiniemi et al., 2013; Whitney et al., 2017). Direct cell-to-cell toxin delivery was first discovered in *Escherichia coli* isolate EC93, which uses a specialized type V secretion system – comprised

of the CdiB and CdiA proteins – to inhibit the growth of other *E. coli* strains in a process termed contact-dependent growth inhibition or CDI (Aoki et al., 2005). CdiB is an Omp85 β-barrel transport protein that exports the CdiA effector across the outer membrane. During its biogenesis, CdiA undergoes a programmed secretion arrest that sequesters the C-terminal half of the effector in the periplasm (Ruhe et al., 2018). The N-terminal half of CdiA forms an extracellular filament that projects ~33 nm from the cell surface (Ruhe et al., 2018). The distal tip of the filament contains an adhesin domain that recognizes a specific receptor on target *E. coli* cells. Once receptor is engaged, CdiA export resumes, and the C-terminal toxin region (CdiA-CT) is transferred into the target bacterium. The CdiA-CT toxin from *E. coli* EC93 forms membrane pores, which dissipate the proton gradient and interfere with ATP synthesis in target bacteria (Aoki et al., 2009). The *cdi* locus also encodes a small CdiI immunity protein that neutralizes CdiA-CT activity to protect the cell from auto-intoxication (Aoki et al., 2005). Thus, CDI allows *E. coli* EC93 cells to inhibit non-isogenic competitors, while simultaneously providing immunity to the toxins delivered by siblings.

Genome surveys reveal that *cdi* loci are wide-spread throughout Gram-negative species and are particularly common in pathogenic proteobacteria (Aoki et al., 2010; Willett et al., 2015b; Zhang et al., 2012). A hallmark of CDI systems is the striking polymorphism of CdiA-CT and CdiI sequences across bacteria. Different isolates of a given species often deploy distinct toxin domains, which are encoded together with equally unique immunity proteins (Anderson et al., 2012; Aoki et al., 2010; Nikolakakis et al., 2012). The variable CdiA-CT region is usually demarcated by a conserved peptide motif, exemplified by the VENN sequence in enterobacteria. We currently recognize 130 CdiA-CT sequence types and note that toxin-immunity pairs within the same family can exhibit significant sequence variation. These latter polymorphisms are concentrated at the CdiA-CT•CdiI binding interface, and therefore immunity proteins generally do not provide cross-protection against "near-cognate" toxins (Michalska et al., 2018; Morse et al., 2015; Poole et al., 2011). CDI system evolution is also heavily influenced by horizontal gene transfer. *E. coli cdi* loci are invariably located within genomic islands or on plasmids, and the 3′-regions are frequently littered with fragmented *cdiA-CT/cdiI* sequences and interspersed integrase and transposase genes (Aoki et al., 2010; Poole et al., 2011; Ruhe et al., 2016). These observations suggest that bacteria acquire new *cdiA-CT/cdiI* sequences via horizontal gene transfer and integrate the modules into the *cdi* locus to change the toxin they deploy (Arenas et al., 2013; Poole et al., 2011). This hypothesis is supported by experimental work showing that *cdiA-CT/cdiI* modules from various species can be fused at the VENN coding sequence of *cdiA* from *E. coli* EC93 to produce functional chimeras (Aoki et al., 2010; Beck et al., 2014; Webb et al., 2013; Willett et al., 2015a). Together, these observations suggest that novel toxins confer a selective advantage, which in turn drives the rapid diversification and exchange of toxin-immunity gene pairs. In this manner, CDI toxin-immunity protein diversity contributes to self-nonself recognition, allowing bacteria to establish kin groups that ultimately shape the structure of microbial communities (Anderson et al., 2012, 2014).

Though there are more than a hundred CDI toxin sequence types, only 42 have predicted biochemical activities and/or functional annotations (Table S1). Some CdiA-CT sequences are clearly related to the C-terminal nuclease domains of colicins, which are diffusible protein toxins released by many strains of *E. coli* (Cascales et al., 2007). CdiA proteins from

Erwinia chrysanthemi EC16 (NCBI reference: AAN38708.1), *Bordetella petrii* BAA-461 (CAP40933.1), *Burkholderia pseudomallei* K96243 (WP_011205723.1) and *Moraxella catarrhalis* McGHS1 (ABQ43332.1) carry toxins that are homologous to the nuclease domains of colicin E3, colicin D, colicin E5 and colicin E2, respectively (Table S1) (Aoki et al., 2010; Walker et al., 2004). Biochemical analyses have confirmed that CdiA-CT^{EC16} cleaves 16S rRNA at the same site as colicin E3, and that CdiA-CT^{K96243} cleaves the anticodon loops of queuosine-containing tRNAs in the same manner as colicin E5 (Beck et al., 2014; Nikolakakis et al., 2012). Aravind and coworkers have identified numerous novel toxin (Ntox) families, many of which are associated with CDI systems and are predicted to have RNase activities (Table S1) (Zhang et al., 2012; Zhang et al., 2011). Of these, the Ntox21 (Pfam: PF15526), Ntox28 (PF15605) and EndoU (PF14436) families have been confirmed experimentally. The Ntox21 domain has the same fold and 16S rRNA nuclease activity as colicin E3 (Beck et al., 2014; Zhang et al., 2012). The Ntox28 domain forms a small α-helical bundle that cleaves the anticodon loops of several tRNAs (Aoki et al., 2010; Diner et al., 2012; Johnson et al., 2016a). The EndoU domain resembles eukaryotic and viral RNA processing enzymes (Holberger et al., 2012; Jamet et al., 2015; Michalska et al., 2018; Zhang et al., 2012). Most of the remaining annotated CDI toxin types are predicted to be DNases and nucleobase deaminases (Table S1) (Zhang et al., 2012), though these activities have yet to be verified experimentally.

Given that most CdiA-CT domains lack functional annotations, we have used a combination of crystallography and biochemical approaches to identify new toxin activities and provide insight into the diversity of toxin-immunity protein interactions. This work has revealed that many CDI toxins adopt known nuclease folds. CdiA-CT domains from *B. pseudomallei* strains 1026b and 1655 share the core α/β-fold of PD(D/E)-XK superfamily phosphodiesterases (Johnson et al., 2016b; Morse et al., 2012; Nikolakakis et al., 2012). This fold forms the catalytic core of restriction endonucleases, but the *Burkholderia* CDI toxins are specific for tRNA. CdiA-CT^{Ykris} from *Yersinia kristensenii* ATCC 33638 is the first RNase A superfamily member to be found outside of vertebrates, though the toxin shares no detectable sequence similarity with RNase A orthologs and lacks the superfamily's characteristic disulfide bonds (Batot et al., 2017). Finally, CdiA-CT^{NC101} from *E. coli* NC101 is a member of the Barnase/EndoU/colicin E5-D/RelE (BECR) RNase family. This latter toxin is remarkable because it requires the essential translation factors EF-Tu and EF-Ts to cleave tRNA substrates (Jones et al., 2017; Michalska et al., 2017). In each instance, computational approaches did not predict that the toxin domains were related to known nuclease families, underscoring the inherent difficulty in predicting structure and function solely from protein sequence. Based on these examples, it seems likely that many uncharacterized CDI toxins belong to known enzyme families.

Here, we extend our survey to CdiA-CT•CdiI complexes from *E. coli* 3006 (EC3006) and *Klebsiella pneumoniae* 342 (Kp342). Position-specific iterated (PSI) BLAST analysis suggests that these toxin domains are related, though they only share ~13% sequence identity. Crystal structures of the complexes support this relationship, revealing that the C-terminal subdomain of each toxin adopts the BECR RNase fold. However, the corresponding immunity proteins are completely unrelated in sequence and structure. The toxins are structurally similar to the tRNase domain of colicin D, which cleaves the anticodon loops of

tRNA^{Arg} isoacceptors (Tomita et al., 2000). Though CdiA-CT^{Kp342} and CdiA-CT^{EC3006} are also isoacceptor specific tRNases, they cleave the aminoacyl acceptor stem of tRNA$_{GAU}^{Ile}$. Further, purified CdiA-CT^{EC3006} alone is sufficient to cleave tRNA$_{GAU}^{Ile}$ *in vitro*, whereas CdiA-CT^{Kp342} requires translation factors EF-Tu and EF-Ts for its activity. The dramatically different structures of CdiI immunity proteins, together with the differential requirement for EF-Tu and EF-Ts, strongly suggest that these BECR RNase domains are related through convergent evolution.

Results

Crystallization and structure determination

We cloned the *cdiA-CT* and *cdiI* coding sequences from *K. pneumoniae* 342 and *E. coli* 3006 into T7 RNA polymerase expression plasmids. Each CdiA-CT construct includes the VENN peptide motif, which begins at Val2905 in CdiA^{Kp342} and Val2921 in CdiA^{EC3006} (Figure S1). To facilitate comparisons of homologous toxins carried by different CdiA effectors, CdiA-CT residues are typically numbered from Val1 of the conserved VENN motif. The CdiA-CT•CdiI^{Kp342} complex has the wild-type sequence, but CdiA-CT^{EC3006} lacks residue Asn332, for which the codon was inadvertently deleted during PCR amplification. Protein complexes were labeled with selenomethionine and purified by Ni^{2+}-affinity chromatography using His_6 epitope tags appended to the N-terminus of CdiA-CT^{Kp342} and the C-terminus of CdiI^{EC3006}. Prior to crystallization, both complexes were subjected to limited proteolysis, which removed the N-terminal "cytoplasm-entry" domain from each CdiA-CT construct (Figure S1). Cytoplasm-entry domains have no toxin activity, but are required to translocate the toxin across the cytoplasmic membrane of target bacteria (Willett et al., 2015a). The CdiA-CT•CdiI^{Kp342} complex crystallized in space group $P2_12_12$ with two heterotetrameric complexes in the asymmetric unit (Table 1). CdiA-CT•CdiI^{EC3006} crystallized in space group $P2_1$ with two heterodimeric complexes in the asymmetric unit (Table 1). Structures were determined at 2.55 Å for CdiA-CT•CdiI^{Kp342} and 2.20 Å for CdiA-CT•CdiI^{EC3006} by SAD phasing using anomalous signals from selenium atoms.

Structure of the CdiA-CT•CdiI^{Kp342} complex

CdiA-CT^{Kp342} and CdiI^{Kp342} form a heterotetrameric complex in the crystal with two toxin domains bound to each CdiI^{Kp342} homodimer (Figure 1A). The crystallized toxin domain (chains A, C, E and G) likely spans residues Val139 – Lys264, with the most complete chain containing residues Thr143 – Gly261 (chain E). The CdiA-CT^{Kp342} toxin domain consists of four N-terminal α-helices and a four-stranded antiparallel β-sheet at the C-terminus (Figure 1A). The β-sheet is twisted and partially wraps around helix α4. All CdiI^{Kp342} immunity proteins (chains B, D, F and H) are nearly complete. Each heterotetramer is covalently linked to its crystallographic symmetry mate through a disulfide bond between CdiI^{Kp342} residue Cys38. This linkage is likely an artifact of crystallization, because the CdiA-CT•CdiI^{Kp342} complex migrates as a tetramer, not an octamer, during size-exclusion chromatography (data not shown). CdiI^{Kp342} forms a dimeric β-sandwich with each protomer contributing two antiparallel β-sheets (Figure 1A). The N-terminal (β1′-β5′) and C-terminal (β6′-β9′) sheets from each protomer interact in parallel via β5′ and β9′ to form a 9-stranded mixed β-sheet (Figure 1B). In addition to the β-complementation H-bond

network, the backbone amides of Lys93 make direct H-bond contacts with the side-chains of Glu94, and the amide side-chains of Asn97 also interact with one another across the dimer interface (Figure 1B).

The CdiA-CT•CdiI^{Kp342} binding interface buries ~1,800 Å^2 (on average) of the solvent-accessible surface area. In general, peripheral elements of CdiI^{Kp342} interact with the toxin domain. N-terminal residues Glu4, Lys6 and Glu9 of the immunity protein interact with Lys213, Tyr215 and Tyr219 (respectively) within the β1-β2 hairpin of the toxin domain (Figure 1C). CdiI^{Kp342} residues Arg25 and Asp26 form salt-bridges with Glu244 and Arg252/Lys157 (respectively) in the toxin domain (Figure 1C). The N-terminal β-sheet of CdiI^{Kp342} interacts extensively with the long loop connecting helices α2 and α3 of the toxin. CdiI^{Kp342} Asp70 forms a salt-bridge with toxin residue Arg174, and CdiI^{Kp342} residues Ser22 and Ser29 both bind to His170 in CdiA-CT^{Kp342} (Figure 1C). There are additional hydrophobic contacts between CdiI^{Kp342} residues Phe2, Phe23, Phe30, Val48 and Val49 and CdiA-CT^{Kp342} residues Tyr215, Tyr219 and Phe222 within the β1-β2 hairpin.

Structure of the CdiA-CT•CdiI^{EC3006} complex

The CdiA-CT•CdiI^{EC3006} asymmetric unit contains two heterodimeric complexes. The modeled CdiA-CT^{EC3006} toxin domains (chains A & B) contain residues Asn175 – Lys336 (numbered from Val1 of the VENN peptide motif), and residues Val4 – Asn161 of CdiI^{EC3006} are resolved (chains C & D). The CdiA-CT^{EC3006} toxin domain is composed of a globular α/β-head subdomain, from which extends an α-helical protrusion. The head subdomain is composed of two three-stranded antiparallel β-sheets (β1-β3 and β4-β6) that wrap around helix α5 (Figure 2A). The N-terminal sheet (β1-β3) interacts with the C-terminal sheet (β4-β6) in parallel via β3 and β6. The short helix α1 follows the N-terminal sheet and leads into the long helical extension formed by α2, α3 and α4 (Figure 2A). The CdiI^{EC3006} immunity protein adopts an α-solenoid structure with α1′-α2′, α3′-α4, α5′-α6′ and α7′-α8′ forming α-hairpins, of which the latter two are linked by short 3_{10} helices, G1′ and G2′ (Figure 2A).

CdiI^{EC3006} binds between the two subdomains of CdiA-CT^{EC3006} through an extended network of direct H-bonds and salt-bridges. The primary anchoring interactions link the internal helical layer (α2′, α4′ and α6′) of CdiI^{EC3006} to the α-helical protrusion of the toxin. Many of these contacts involve toxin helix α4, with residues Glu249 and Glu252 both interacting with Lys103 of CdiI^{EC3006} (Figure 2B). Toxin residue Arg260 forms a salt bridge with Asp140 of CdiI^{EC3006} (Figure 2B). In addition, the loop connecting α1′ to α2′ of CdiI^{EC3006} inserts into the cleft between the β-sheets of the toxin α/β-head subdomain (Figure 2B). The main-chain carbonyl groups of Ala25, Asn26 and Phe28 in this loop interact with the amide backbone of Ala185 and the side-chain of Lys204, respectively (Figure 2B). The side-chains of CdiI^{EC3006} residues Asn26, Asn62 and Asp140 also form direct H-bonds with toxin residues Arg327, Arg299 and Thr334, respectively (Figure 2B). Hydrophobic contacts further stabilize the complex, with immunity protein residues Phe67, Phe143 and Tyr144 stacking against the toxin in the vicinity of Lys253, His256 and Arg260. Altogether, the CdiA-CT•CdiI^{EC3006} interface buries ~4,300 Å^2 of the solvent-accessible surface area of the monomeric units.

CdiA-CT^{Kp342} and CdiA-CT^{EC3006} are structurally similar

Although CdiA-CT^{Kp342} and CdiA-CT^{EC3006} share only ~13% sequence identity, each is captured by iterative PSI-BLAST search when the other domain is submitted as the query (Table S2). In accordance with this sequence similarity, the CdiA-CT^{Kp342} structure superimposes onto the α/β-head subdomain of CdiA-CT^{EC3006} with rmsd of 2.7 Å (Figure 3A). The toxins share the C-terminal β-sheet, though this element consists of four strands in CdiA-CT^{Kp342}. CdiA-CT^{Kp342} helices α2 and α4 correspond to α1 and α5 in CdiA-CT^{EC3006} (Figures 3B & 3C). The N-terminal β-sheet of CdiA-CT^{EC3006} is replaced by helix α1 in CdiA-CT^{Kp342}, and the α-helical protuberance of CdiA-CT^{EC3006} is significantly reduced to a long loop and short helix α3 in CdiA-CT^{Kp342}. DALI searches for structural homologs of CdiA-CT^{Kp342} and CdiA-CT^{EC3006} recover a number of ribonucleases that share the barnase/EndoU/colicin D-E5/RelE (BECR) fold (Holm and Rosenstrom, 2010; Zhang et al., 2012). The closest structural homologs of CdiA-CT^{Kp342} include the C-terminal domain of colicin D and the BrnT toxin from *Brucella abortus* (Table 2). Intriguingly, we also recovered the CDI toxin from *E. coli* strain NC101 (Table 2), which requires translation factors EF-Tu and EF-Ts to cleave tRNA substrates *in vitro* (Michalska et al., 2017). Hits from the CdiA-CT^{EC3006} search were dominated by proteins that superimpose onto the α-helical extension subdomain, and only four of the top several hundred hits match the α/β-head subdomain. These include type II ParE toxins from *Mesorhizobium opportunistum, E. coli* O157:H7 str. SS52 and *Caulobacter vibrioides* (Table 2). Thus, the CdiA-CT^{Kp342} and CdiA-Ct^{EC3006} toxin domains are heretofore unrecognized members of the BECR ribonuclease superfamily.

In contrast to the toxin domains, the immunity proteins are unrelated in sequence and structure (Figures 3B & 3C). The β-sandwich module of CdiI^{Kp342} is present in several bacterial enzymes, including β-galactosidase and amine oxidases (Table 2). Though this β-motif is common in various proteins, CdiI^{Kp342} appears to be the first example of an immunity protein with this fold. The DALI search for CdiI^{EC3006} homologs recovered several eukaryotic proteins with armadillo-like repeats (Figure 2A). These latter structural homologs include a subunit of the clathrin associated AP-1 complex, human importin and transportin proteins that function in nuclear import, and the yeast RNA-scaffolding protein Puf5p (Table 2). Although the CdiI proteins are structurally distinct, both bind to their cognate toxins at the same relative position on the α/β core (Figures 3B & 3C), suggesting that they neutralize their cognate toxins using similar mechanisms.

CdiA-CT^{EC3006} and CdiA-CT^{Kp342} cleave tRNA$_{GAU}^{Ile}$

We previously showed that tRNA$_{GAU}^{Ile}$ is cleaved in response to CdiA-CT^{EC3006} intoxication (Willett et al., 2015a). Given the structural homology between CdiA-CT^{EC3006} and CdiA-CT^{Kp342}, we tested whether the toxins also exhibit similar tRNase activities. We co-expressed each toxin with cognate CdiI that carries a C-terminal ssrA(DAS) degron (McGinness et al., 2006). Degron-tagged immunity proteins are degraded by the ClpXP protease, thereby liberating the toxins to act on cellular substrates. We note that wild-type CdiA-CT^{EC3006} (containing Asn332) was used for this and all following experiments. Northern blot analysis confirmed that CdiA-CT^{EC3006} activation leads to tRNA$_{GAU}^{Ile}$ cleavage (Figure 4A, compare lanes 1, 2 & 3). This activity is specific, because no cleavage

of $tRNA_{UAC}^{Val}$, $tRNA_{GUA}^{Tyr}$ or $tRNA_{UAA}^{Leu}$ was detected (Figure 4A). Analysis of RNA from CdiA-CT^{Kp342} intoxicated cells revealed similar RNase activity and substrate specificity (Figure 4A, compare lanes 1, 4 & 5), suggesting that both toxins are isoacceptor specific tRNases.

Though CdiA-CT^{Kp342} and CdiA-CT^{EC3006} have similar activities, Northern blot analysis lacks the resolution to determine whether the toxins cleave substrate at the same positions. Because other CDI toxins degrade the 3′-ends of tRNA (Jones et al., 2017; Michalska et al., 2017; Nikolakakis et al., 2012), we used S1 nuclease protection analysis to map cleavage sites in the 3′-arm of the aminoacyl acceptor stem (Figure 4B). This analysis revealed that $tRNA_{GAU}^{Ile}$ is truncated after nucleotide C72 in CdiA-CT^{Kp342} intoxicated cells (Figures 4C, lanes 3 & 4). CdiA-CT^{EC3006} also acts on the acceptor stem, but cleaves after nucleotide C71 (Figures 4D, lanes 3 & 4). These cleaved tRNAs cannot be repaired by the CCA-adding nucleotidyl transferase, because the unpaired discriminator nucleotide is removed (Betat et al., 2010). Thus, both toxins inactivate $tRNA_{GAU}^{Ile}$ by releasing short 3′-oligonucleotide fragments.

tsf mutants are resistant to CdiA-CT^{Kp342}, but not CdiA-CT^{EC3006} intoxication

As noted above, CdiA-CT^{Kp342} shares structural homology with the CdiA-CT^{NC101} toxin domain from *E. coli* NC101. CdiA-CT^{NC101} requires translation factors EF-Tu and EF-Ts to support its tRNase activity *in vitro*; and *tsf* mutations that alter the coiled-coil domain of EF-Ts protect target bacteria from inhibition by this toxin (Michalska et al., 2017). Therefore, we tested *tsf* mutants for resistance to CdiA-CT^{Kp342} and CdiA-CT^{EC3006} to determine whether the toxins are translation factor-dependent. We first fused CdiA-CT^{Kp342} and CdiA-CT^{EC3006} sequences to the VENN motif of $CdiA^{EC93}$ and confirmed that the resulting chimeras are active in competition co-cultures. Cells expressing the chimeric effectors outcompete wild-type target bacteria ~1,000-fold after 1 h of co-culture in shaking broth (Figure 5A). This growth advantage is due to CdiA-CT toxin activity, because competitive fitness is restored to target cells that express cognate *cdiI*, whereas non-cognate immunity genes are not protective (Figure 5A). We then examined *tsf(A202E)* and *tsf(Δcoil)* target cells, which encode EF-Ts with an Ala202Glu substitution at the tip of the coiled-coil domain and a deletion of the entire coiled-coil domain, respectively. Both *tsf* mutants are completely resistant to inhibition by CdiA-CT^{Kp342}, but remain as susceptible to CdiA-CT^{EC3006} intoxication as tsf^+ target bacteria (Figure 5A). We also used Northern blotting to monitor toxin activity in the co-cultures. Cleaved $tRNA_{GAU}^{Ile}$ was readily detected in RNA isolated from co-cultures with non-immune tsf^+ target bacteria (Figure 5B, lanes 1 & 6). Because these co-cultures were seeded with inhibitor and target cells at a 1:1 ratio, only half of the $tRNA_{GAU}^{Ile}$ should be cleaved because inhibitor bacteria are immune to their own toxin. Accordingly, the expression of cognate *cdiI* in target cells blocked this nuclease activity (Figure 5B, lanes 4 & 10). Together, these observations indicate that the toxins degrade most, if not all, tRNA substrate in target cells. S1 protection analysis confirmed that $tRNA_{GAU}^{Ile}$ is cleaved at the same sites identified from intra-cytoplasmic expression (Figures 4C & 4D, lanes 5 & 6). Analysis of RNA isolated from co-cultures with *tsf* target bacteria revealed that CdiA-CT^{EC3006} retains full tRNase activity (Figure 5B, lanes 2 & 3), whereas the CdiA-CT^{Kp342} toxin appears to be inactive in these target cells (Figure 5B,

lanes 7 & 8). Thus, wild-type EF-Ts is required for CdiA-CT^{Kp342} mediated nuclease activity and cell killing, but has no influence on intoxication by CdiA-CT^{EC3006}.

CdiA-CT^{Kp342} and CdiA-CT^{C3006} are specific for deacylated tRNA^{Ile}

To confirm that CdiA-CT^{Kp342} and CdiA-CT^{EC3006} directly catalyze tRNA cleavage, we tested the nuclease activities of purified toxin domains *in vitro*. Initial experiments with CdiA-CT^{EC3006} showed that only a fraction of the tRNA$_{GAU}^{Ile}$ substrate in total RNA preparations is cleaved (Figure 6A). We attempted to optimize the reactions using different buffers and Mg^{2+} supplementation, but still found that about half of the substrate could be converted (Figure 6A). Given that CdiA-CT^{EC3006} cleaves near the 3′-end of tRNA$_{GAU}^{Ile}$, we reasoned that aminoacylation may affect substrate selection. Using acid-urea gel electrophoresis to resolve aminoacylated from deacylated tRNAs, we found that about half of the tRNA$_{GAU}^{Ile}$ is charged in total RNA isolated from *E. coli* (Figure 6B, lane 1). Analysis of *in vitro* nuclease reactions on acid-urea gels revealed that CdiA-CT^{EC3006} preferentially cleaves the deacylated fraction of tRNA$_{GAU}^{Ile}$ (Figure 6B, compare lanes 1 & 2). This activity is not due to contaminating RNases, because it can be blocked with purified CdiI^{EC3006} (Figure 6B, lane 3). Based on these results, we repeated the *in vitro* nuclease assays with deacylated tRNA and found that this substrate was cleaved efficiently by CdiA-CT^{EC3006} (Figure 6C, lanes 1 & 2). Though CdiA-CT^{EC3006} is specific for tRNA$_{GAU}^{Ile}$ *in vivo*, we detected significant activity against tRNA$_{UAC}^{Val}$ and tRNA$_{UAA}^{Leu}$ *in vitro* (Figure 6C). In contrast to CdiA-CT^{EC3006}, purified CdiA-CT^{Kp342} shows weak tRNase activity *in vitro* (Figure 6C, lanes 4 & 5). Because *tsf* mutants are resistant to CdiA-CT^{Kp342}, we reasoned that this toxin probably requires EF-Tu and EF-Ts for full nuclease activity. Indeed, supplementation with purified EF-Tu and EF-Ts greatly stimulates CdiA-CT^{Kp342} activity *in vitro* (Figure 6C, compare lanes 4 & 6). Both translation factors are required for nuclease activity, because CdiA-CT^{Kp342} does not cleave substrate in reactions supplemented with either EF-Ts or EF-Tu individually (Figure 6D, lanes 3 & 4). The activity is also GTP-dependent (Figure 6D, compare lanes 5 & 6), suggesting that CdiA-CT^{Kp342} recognizes its substrate in the context of tRNA•EF-Tu•GTP ternary complexes. Further, we found that translation factor-activated CdiA-CT^{Kp342} only cleaves deacylated tRNA$_{GAU}^{Ile}$ *in vitro* (Figure 6B, lane 4).

The toxins' specificity for uncharged tRNA is unusual and perhaps unprecedented. This finding is particularly surprising for CdiA-CT^{Kp342}, because this toxin presumably acts on tRNA•EF-Tu•GTP, and EF-Tu has relatively low affinity for uncharged tRNA (Janiak et al., 1990). Therefore, we asked whether deacylated tRNA is a relevant substrate inside target bacteria. We first treated *E. coli* target bacteria with the antibiotic mupirocin – which inhibits isoleucyl-tRNA synthetase (Yanagisawa et al., 1994) – to convert all cellular tRNA$_{GAU}^{Ile}$ into the deacylated form (Figure 6E). We then introduced mupirocin-resistant inhibitor cells that deploy CdiA-CT^{EC3006} or CdiA-CT^{Kp342} and incubated the mixed populations for 30 min in the presence of mupirocin. Northern blot analysis revealed tRNase activity in the co-cultures with mupirocin-treated target cells that lack immunity (Figure 6F). Moreover, cleaved tRNA$_{GAU}^{Ile}$ levels were roughly equivalent to those observed in co-cultures without mupirocin treatment (compare Figure 6F, lanes 1 & 3 with Figure 5B, lanes 1 & 6),

indicating that the antibiotic has no discernable effect on toxin activity *in vivo*. Taken together, these results demonstrate that both toxins are specific for deacylated $tRNA_{GAU}^{Ile}$.

The nuclease active sites of CdiA-CT^{Kp342} and CdiA-CT^{EC3006}

Finally, we probed the active site of each toxin domain to gain insight into catalysis. BECR RNases are diverse and use a variety of catalytic residues to cleave substrate (Zhang et al., 2014). We chose colicin D as a model to guide mutagenesis because its C-terminal nuclease domain is the closest structural homolog of CdiA-CT^{Kp342} (Table 2), and its active site has been examined in detail (Graille et al., 2004). Structure superimposition shows that CdiA-CT^{Kp342} residues Lys157, Tyr160 and Thr255 are arranged in the same relative positions as catalytic residues Lys608, His611 and Ser677 in colicin D (Figure 7A). The CdiA-CT^{EC3006} toxin appears to have a similarly configured active site with residues Lys204, Tyr208 and Thr330 (Figure 7B). In addition, Arg174 and Arg252 of CdiA-CT^{Kp342} superimpose with CdiA-CT^{EC3006} Arg260 and Arg327 (respectively) (Figure 7B), suggesting that they may contribute to substrate binding. The putative catalytic triad of CdiA-CT^{Kp342} is completely conserved between close homologs (Figure S2), whereas homologs of CdiA-CT^{EC3006} sometimes contain Phe or Trp residues in place of Tyr208 (Figure S3). CdiA-CT^{Kp342} homologs also contain an invariant His170 residue directed toward the putative active site, and this residue may be equivalent to His256 in CdiA-CT^{EC3006} (Figures S2 & 7B). We first mutated these residues in the context of full-length CdiA chimeras to examine the effects on growth inhibition activity in competition co-cultures. Ala substitutions of CdiA-CT^{Kp342} residues Lys157, Tyr160 and Arg252 completely abrogate inhibition activity (Figure 7C). Mutation of His170 and Thr255A significantly attenuated growth inhibition activity, whereas the Arg174Ala mutation had no discernable effect (Figure 7C). Similar results were obtained with the corresponding mutations made in the CdiA-CT^{EC3006} domain, though the Arg260Ala mutation abrogates CdiA-CT^{EC3006} inhibition activity (Figure 7D). We note that each CdiA variant is produced at the same level as wild-type (Figure S4), indicating that functional defects are not the result of low expression or protein destabilization. Northern blot analyses of RNA from these co-cultures showed that inhibition activities are closely correlated with $tRNA_{GAU}^{Ile}$ cleavage in target bacteria (Figures 7E & 7F). To further test whether the mutations directly influence nuclease activity, we purified the CdiA-CT^{EC3006} variant toxin domains and examined their activities on deacylated tRNA *in vitro*. Overall, CdiA-CT^{EC3006} *in vitro* activity correlates well with the competitive fitness of inhibitor bacteria. For example, the Glu236Ala substitution has no apparent effect on competitive fitness (Figure 7D) and the corresponding purified CdiA-CT has the same nuclease activity as wild-type *in vitro* (Figure 7G). Taken together, these results indicate that the mutations directly affect tRNase activity, either by interfering with substrate binding or catalysis.

Discussion

The C-terminal toxin domains of CdiA^{Kp342} and CdiA^{EC3006} share structural homology, and both are specific tRNases that cleave the acceptor stem of $tRNA_{GAU}^{Ile}$. In contrast, the CdiI^{Kp342} and CdiI^{EC3006} immunity proteins differ radically in both sequence and structure, suggesting that the similarities between their cognate toxins arose through convergent evolution. Because immunity protein function is essential to protect toxin producing cells

from self-inhibition, toxin-immunity gene pairs are thought to evolve through iterative mutation cycles in which substitutions that perturb complex formation are compensated by reciprocal changes in the cognate partner that reestablish binding affinity (Morse et al., 2015; Riley, 1993a, b). This phenomenon is apparent in alignments of CdiA-CT•CdiI^{Kp342} and CdiA-CT•CdiI^{EC3006} with homologous toxin-immunity protein pairs from other bacterial species (Figures S2 & S3). For example, toxin-interacting residues within CdiI^{EC3006} are not conserved between close homologs (Figure S3B). The predicted immunity proteins for CdiA-CT^{Kp342} homologs exhibit even greater variability, with no significant identity shared by CdiI^{Kp342} and the *Pseudomonas* immunity proteins in Figure S2B. This latter observation shows that immunity protein sequences can diverge radically during evolution. Nevertheless, each immunity protein in Figure S2B has the same predicted secondary structure as CdiI^{Kp342}, suggesting that all fold into dimeric β-sandwiches. The fact that CdiI^{EC3006} does not share this predominately β fold strongly suggests that it, and its cognate toxin domain, evolved from a different primordial ancestor than the CdiA-CT•CdiI^{Kp342} complex.

CdiA-CT^{Kp342} and CdiA-CT^{EC3006} also differ in their requirements for extrinsic activation. Purified CdiA-CT^{EC3006} is competent to cleave substrate *in vitro*, but CdiA-CT^{Kp342} activity is dependent on translation factors EF-Tu and EF-Ts. Perhaps the unique α-helical subdomain in CdiA-CT^{EC3006} contributes to substrate binding, and this function is fulfilled by EF-Tu/EF-Ts for CdiA-CT^{Kp342}. CDI toxins from *E. coli* EC869 and *E. coli* NC101 also require EF-Tu and EF-Ts for activity (Jones et al., 2017; Michalska et al., 2017). These latter toxins also cleave the 3′-ends of specific tRNAs and are thought to use EF-Tu as a scaffold to position substrate in their active sites. Structures of the EF-Tu•CdiA-CT•CdiI^{NC101} complex show that the toxin binds to domain 2 of EF-Tu at a position that partially overlaps with the aminoacylated-tRNA binding site (Michalska et al., 2017). Though CdiA-CT^{Kp342} and CdiA-CT^{NC101} do not share significant sequence homology, they have similar tertiary structures (see Table 2), raising the possibility that they bind EF-Tu in the same manner. However, the CdiA-CT^{Kp342} toxin clashes with several elements of EF-Tu when modeled in place of CdiA-CT^{NC101} in the EF-Tu•CdiA-CT•CdiI^{NC101} crystal structure. Helix α4 of CdiA-CT^{Kp342} interferes with EF-Tu strand e2, and there are clashes between the a2-b2 hairpin of the translation factor and α5, β2 and β3 of the toxin (Figure S5). Therefore, CdiA-CT^{Kp342} and CdiA-CT^{NC101} presumably interact with EF-Tu using distinct contacts, consistent with differences in their cleavage sites on tRNA. CdiA-CT^{Kp342} cleaves within the double-stranded acceptor stem, whereas CdiA-CT^{NC101} removes the single-stranded 3′ tail from substrate tRNA (Michalska et al., 2017). CdiA-CT^{Kp342} and CdiA-CT^{NC101} also differ in their responses to aminoacylated substrate. CdiA-CT^{NC101} appears to act on both aminoacylated and deacylated tRNAs, whereas CdiA-CT^{Kp342} activity is blocked by aminoacylation. The latter result is surprising because EF-Tu-dependent toxins are presumed to recognize substrate in the context of tRNA•EF-Tu•GTP ternary complexes, and EF-Tu binds deacylated tRNA with ~10^3-fold lower affinity than aminoacyl-tRNA (Janiak et al., 1990). Nonetheless, we find that a substantial proportion of $tRNA_{GAU}^{Ile}$ is deacylated in *E. coli* cells (see Figure 6A), and this substrate is rapidly degraded upon intoxication with CdiA-CT^{Kp342}. These observations suggest that EF-Tu binds deacylated tRNA *in vivo*. In principle, this interaction could be driven by mass action, because the intracellular

concentration of EF-Tu (~50 μM) is about 20-fold higher than the dissociation constant (~2.5 μM) for binding to deacylated tRNA. Alternatively, EF-Tu may promote nuclease activity independent of its tRNA-binding properties, perhaps functioning as a chaperone to stabilize the toxin. We note that translation factors are not intrinsically required for acceptor-stem tRNase activity, because CdiA-CT^{EC3006} catalyzes a similar reaction in the absence of EF-Tu and EF-Ts.

To our knowledge, CdiA-CT^{Kp342} and CdiA-CT^{EC3006} are the first RNases reported to act specifically on tRNA$_{GAU}^{Ile}$. Though this substrate specificity is novel, other isoacceptor specific tRNases have been identified over the past 30 years and several of these nucleases mediate interbacterial competition. Colicins E5 and D are diffusible protein toxins released by certain strains of *E. coli* to kill non-isogenic competitors (Cascales et al., 2007). Colicin E5 carries a C-terminal tRNase domain that cleaves the anticodon loops of tRNA^{Asn}, tRNA^{Asp}, tRNA^{His} and tRNA^{Tyr} (Ogawa et al., 1999). Similarly, colicin D carries an anticodon nuclease domain that is specific for tRNA^{Arg} isoacceptors (Tomita et al., 2000). We note that the colicin D nuclease domain is the closest known structural homolog of CdiA-CT^{Kp342}, demonstrating that the BECR fold can adapt to recognize different tRNA subdomains. Other CdiA effectors also deliver toxic tRNase domains. CdiA^{Bp1026b} from *B. pseudomallei* 1026b carries a C-terminal PD-(D/E)XK phosphodiesterase domain that preferentially cleaves the acceptor stem of tRNA^{Ala} (Koskiniemi et al., 2013; Nikolakakis et al., 2012), and the EndoU RNase domain in CdiA^{STECO31} from *E. coli* STEC_O31 is a tRNA^{Glu} specific anticodon nuclease (Michalska et al., 2018). Specific tRNase toxins are also deployed for inter-strain competition between Gram-positive bacteria. The large cell wall-associated proteins (WapA) of *Bacillus subtilis* are functionally analogous to CdiA effectors and inhibit neighboring bacteria with their C-terminal toxin domains. The WapA toxin domain from *B. subtilis* subsp. 'natto' cleaves tRNA^{Glu} in a similar manner as the CdiA-CT^{STECO31} toxin, and the toxin from *B. subtilis* subsp. *spizizenii* T-UB-10 cleaves the tRNA^{Ser} anticodon (Koskiniemi et al., 2013). Isoacceptor specific tRNases also play roles beyond competition. *E. coli* PrrC was the first isoacceptor specific anticodon nuclease to be discovered, and this intriguing enzyme functions as a type of innate immunity to viral infection (Levitz et al., 1990). PrrC is a latent anticodon nuclease that is activated in response to bacteriophage T4 infection to cleave tRNA^{Lys}. This activity blocks protein synthesis, thereby inhibiting phage production to protect neighboring sibling cells that have yet to become infected. More recently, type II proteic toxin-antitoxin (TA) loci have been discovered to encode specific anticodon nucleases. The biological functions of type II TA systems remain enigmatic despite considerable research over the past two decades, but prevailing models postulate that these toxins regulate bacterial growth in response to environmental cues (Gerdes and Maisonneuve, 2012; Van Melderen, 2010). VapC toxins from *Salmonella* and *Shigella* inactivate initiator tRNA$_i^{Met}$ to arrest protein synthesis (Winther and Gerdes, 2011), and the numerous VapC paralogs of *Mycobacterium tuberculosis* exhibit specificities for tRNA^{Ala}, tRNA^{Cys}, tRNA^{Leu}, tRNA^{Gln}, tRNA^{Ser} and tRNA^{Trp} (Cruz et al., 2015; Winther et al., 2016). Finally, the MazF-mt9 toxin from *M. tuberculosis* was recently shown to have tRNA^{Lys} specific anticodon nuclease activity (Schifano et al., 2016). The growing number of isoacceptor specific nucleases underscores the critical role of tRNA in the control of bacterial growth and viability.

CdiA proteins are characterized by their variable C-terminal toxin domains, which can be exchanged between effectors to produce functional chimeras (Aoki et al., 2010; Nikolakakis et al., 2012). This modularity allows the cell to periodically change the toxin it deploys through genetic recombination. Metagenomic analyses strongly suggest that new *cdiA-CT/cdiI* gene pairs are acquired through horizontal gene transfer and fused to *cdiA* via homologous recombination or site-specific integrase activity (Arenas et al., 2013; Poole et al., 2011). Thus, closely related toxin domains are often found distributed across phylogenetically diverse species. This is illustrated in database searches for CdiA-CT^{Kp342} and CdiA-CT^{EC3006} homologs, which return CdiA proteins from several different species. For example, CdiA-CT^{Kp342} homologs are found in predicted CdiA effectors from *Yersinia, Dickeya, Achromobacter, Pseudomonas* and *Burkholderia* species (Table S2 & Figure S2). CdiA-CT^{Kp342} and CdiA-CT^{EC3006} homologs are also commonly found at the C-terminus of Rhs/YD-peptide repeat proteins (Table S2), which constitute another important group of anti-bacterial effectors. In Gram-negative bacteria, Rhs proteins are exported through type VI secretion systems (T6SS) by virtue of their non-covalent interactions with VgrG (Hachani et al., 2014; Koskiniemi et al., 2013; Shneider et al., 2013; Whitney et al., 2014). The Rhs effectors identified in Table S2 are presumably also deployed in a T6SS-dependent manner, because they contain N-terminal PAAR domains, which interact with the C-terminal β-spike of trimeric VgrG (Shneider et al., 2013). The YD-repeat containing WapA protein of *B. subtilis* carries an N-terminal signal peptide for export through the SecYEG translocon (Koskiniemi et al., 2013). In contrast, the *Streptomyces* YD-peptide repeat proteins identified in Table S2 lack recognizable signal peptides, raising the possibility that they are deployed through a specialized secretion system. Lastly, we identified two PrsW metalloproteases from Gram-positive *Paenibacillus* species that carry C-terminal domains that share 32-36% sequence identity with CdiA-CT^{EC3006} (Table S2). PrsW-mediated toxin delivery has yet to be demonstrated experimentally, but their linkage to several polymorphic toxin domain families strongly suggests that these integral membrane proteins function in intercellular competition as first suggested by Aravind and colleagues (Zhang et al., 2012; Zhang et al., 2011).

Finally, this study highlights the limitations of homology modeling to predict protein structure and function. CdiA-CT^{Kp342} and CdiA-CT^{EC3006} are both BECR-fold RNases, yet the domains are not annotated as such in current databases. The BECR superfamily was first defined by Aravind and coworkers, who recognized that the αββββ core of barnase is present in other microbial RNase families (Zhang et al., 2012). In addition to known RNases, Zhang *et al.* also identified 10 uncharacterized toxin subgroups that are predicted to adopt the BECR core fold. These latter novel toxin (Ntox) subgroups are differentiated by distinct sequence motifs that presumably contribute to substrate binding and catalysis. To date, only the Ntox21 group (Pfam: PF15526) has been examined experimentally, and that study confirmed predictions that the domain adopts the BECR fold and cleaves 16S rRNA in the same manner as colicin E3 (Beck et al., 2014; Zhang et al., 2012). Most databases recognize the Ntox35 (PF15534), Ntox47 (PF15540) and Ntox50 (PF15542) BECR groups, but the Ntox7, Ntox19, Ntox36, Ntox41 and Ntox48 families are not listed in the current Pfam 32.0 database. The Ntox48 group may have been misclassified initially, because the CdiA-CT domain from *Dickeya zeae* Ech1591 (NCBI: ACT06855.1) that was originally

cited as the family paragon is now annotated as an EHHH/Endo VII nuclease (PF15657). It is less clear why the remaining five BECR groups are no longer extant. CdiA effectors commonly carry C-terminal Ntox7, Ntox19, Ntox41 and Ntox49 domains, and the CdiA-CT Ntox7 domain from *Y. pestis* Pestoides A inhibits target bacteria when fused to an *E. coli* CdiA protein (Willett et al., 2015a). We note that the diverse active sites of BECR nucleases pose a significant challenge for homology-based predictions. Some BECR nucleases have unusual active sites that lack the canonical His and Glu catalytic residues typically found in RNases. For example, *E. coli* RelE contains no His residues and instead appears to use Lys54 as general base to abstract a proton from the 2′-hydroxyl of its substrate, and Arg81 as an acid to protonate the 5′ leaving group (Dunican et al., 2015; Griffin et al., 2013). Similarly, colicin E5 lacks a catalytic His residue and likely uses Lys or Gln residues to initiate cleavage (Yajima et al., 2006). RelE and colicin E5 also carry unique C-terminal extensions that are critical for substrate recognition (Neubauer et al., 2009; Yajima et al., 2006). BECR active-site plasticity is further compounded by the tendency for catalytic residues to migrate between secondary structure elements (Zhang et al., 2014). The catalytic triad of barnase is contained within the last two strands of the core, but the Lys-His and Lys-Tyr motifs of colicin D and CdiA-CT^{Kp342} emanate from N-terminal α-helices that are not part of the BECR core. Similar structural plasticity is well documented for the PD-(D/E)-XK superfamily of phosphodiesterases, which are notoriously difficult to identify though sequence analysis (Steczkiewicz et al., 2012). We anticipate that many more BECR core variations will be discovered as more superfamily members are identified and characterized.

STAR Methods

Lead contact and materials availability

Further information and requests for resources and reagents should be directed to and will be fulfilled by the Lead Contact, Christopher Hayes (chayes@lifesci.ucsb.edu).

Experimental model and subject details

Bacterial growth conditions.—Bacterial strains are presented in the Key Resources Table. Bacteria were cultured in M9 minimal medium, lysogeny broth (LB) or on LB agar at 37 °C. Unless indicated otherwise, media were supplemented with antibiotics at the following concentrations: 150 μg/mL ampicillin (Amp), 100 μg/mL chloramphenicol (Cm), 50 μg/mL kanamycin (Kan), 200 μg/mL spectinomycin (Spc), and 25 μg/mL tetracycline (Tet).

Method details

Plasmid constructions.—Plasmids are presented in the Key Resources Table and oligonucleotide primers are listed in Table S3.

Protein over-production plasmids: The coding sequences for CdiA-CT/CdiI^{Kp342} and CdiA-CT/CdiI^{EC3006} were synthesized by Genscript (Piscataway, NJ) and supplied in the pUC57 vector (pCH6289 and pCH6283). The *cdiI*^{EC3006} gene was amplified using primers 209CdiIF52/209CdiIR45, and the product inserted into the SspI ligation independent cloning (LIC) site of pMCSG63 (Eschenfeldt et al., 2009; Eschenfeldt et al., 2013) to generate

pMCSG63-APC111476, which produces CdiI^{EC3006} carrying an N-terminal His$_6$ tag. The *cdiA-CT*^{EC006} coding sequence was amplified with primers 209CdiAF43/209CdiAR46, and the product inserted into the SmaI LIC site of plasmid pMCSG63-APC111476. Sequencing revealed that most clones acquired frame-shift mutations that inactivate the toxin gene. One clone (pMCSG63-APC200209) was identified with no frame-shifts, though it contains an in-frame deletion of the codon for Asn332. The *cdiA-CT-cdiI*^{Kp342} module was amplified with primers 215CdiAF41/215CdiIR57, and the product inserted into pMCSG63 as described above to produce plasmid pMCSG63-APC200215, which produces CdiA-CT^{Kp342} with an N-terminal His$_6$ tag and untagged CdiI^{Kp342}.

For biochemical analyses, the *cdiA-CT/cdiI*^{Kp342} and *cdiA-CT/cdiI*^{EC3006} modules were amplified with primers CH3962/CH3685 and CH4304/CH3425 (respectively), and ligated to pCH8001 (Beck et al., 2014) via KpnI/SpeI restriction sites to generate plasmids pCH12861 and pCH978 (respectively). Plasmid sequences were confirmed by DNA sequencing, and therefore wild-type toxins were used for all functional assays. For *in vivo* toxin activation experiments, the *cdiA-CT/cdiI* modules were subcloned into pCH7171 using NcoI/SpeI restriction sites to append ssrA(DAS) degrons onto CdiI^{Kp342} (pCH12158) and CdiI^{EC3006} (pCH13677). The *cdiI*^{Kp342} and *cdiI*^{EC3006} genes were amplified with primers CH3965/CH3685 and CH3244/CH3425 (respectively) and ligated via KpnI/SpeI to pCH8001 to generate plasmids pCH12898 and pCH12802 for the purification of CdiI^{Kp342}-His$_6$ and CdiI^{EC3006}-His$_6$, respectively. The immunity genes were also amplified with CH3965/CH3570 and CH3244/CH3245 (respectively) and ligated to pTrc99aKX via KpnI/XhoI restriction site to generate plasmids pCH12865 and pCH11526, which were used to express native immunity genes in target bacteria during competition co-culture experiments.

Site-directed mutagenesis: Site-directed mutagenesis of *cdiA-CT*^{EC3006} was performed by overlap-extension (OE-PCR) or megaprimer PCR (Aiyar et al., 1996) using primer pair CH4304/CH3425 in conjunction with: CH4276 for Lys204Ala (pCH14301); CH4699/CH4700 for Tyr208Ala (pCH14982); CH4252/CH4253 for His256Ala (pCH13887); CH4250/CH4251 for Glu259Ala (pCH14200); CH4254/CH4255 for Arg260Ala (pCH13888); CH4256/CH4257 for Arg327Ala (pCH14201); and CH4277 for Thr330Ala (pCH13890). All final products were digested with KpnI/SpeI and ligated to pCH8001 to generate protein overexpression constructs. The same general procedure was used introduce site-directed mutations into *cdiA-CT*^{Kp342}. Primer pair CH3962/CH3685 was used in conjunction with CH4438/CH4439 for Lys157Ala; CH4697/CH4698 for Tyr160Ala; CH4440/CH4441 for His170Ala; CH4442/CH4443 for Arg174Ala; CH4444/CH4445 for Arg252Ala; and CH4446/CH4447 for Thr255Ala.

Chimeric CdiA constructions: Chimeric *cdiA*^{EC93}-*CT*^{Kp342} expression constructs were generated by allelic exchange of the counter-selectable *pheS** marker from plasmid pCH10163 (Morse et al., 2012). All *cdiA-CT/cdiI*^{Kp342} alleles were first amplified using primers CH3517/CH3518. The resulting products were fused to DNA fragments amplified from regions upstream and downstream of the *cdiA*^{EC93} gene. The upstream homology fragment was amplified using primers CH4100/CH4101, and the downstream fragment with primers CH4102/CH4103. The upstream and downstream homology fragments were then

fused to *cdiA-CT/cdiI*^{Kp342} modules using OE-PCR with primers CH4100/CH4103. The final DNA products (100 ng) were electroporated together with plasmid pCH10163 (300 ng) into *E. coli* DY378 cells (Thomason et al., 2007). Recombinant clones encoding wild-type (pCH11948), Lys157Ala (pCH14278), Tyr160Ala (pCH14912), His170Ala (pCH14279), Arg174Ala (pCH14280), Arg252Ala (pCH14281), Thr255Ala (pCH14282) alleles of CdiA-CT^{Kp342} were isolated on yeast extract glucose-agar supplemented with 33 μg/mL chloramphenicol and 10 mm D/L-*p*-chlorophenylalanine. The chimeric *cdiA*^{EC93}-*CT*^{EC3006} expression plasmid pCH11483 has been described (Willett et al., 2015a), and derivative constructs encoding Lys204Ala (pCH13892), Tyr208Ala (pCH14913), His256Ala (pCH13893), Glu259Ala (pCH13813), Arg260Ala (pCH13894), Arg327Ala (pCH13895) and Thr330Ala (pCH13896) variants of CdiA-CT^{EC3006} were isolated as described above.

Protein expression, purification and crystallization.—A single colony was inoculated into 2 mL of LB medium supplemented with 100 μg/mL ampicillin and incubated at 37 °C with shaking for 6 h. LB cultures were then diluted 1:100 into 50 mL of M9 medium supplemented with 0.5% glycerol, 100 μg/mL of ampicillin, trace minerals and vitamins. Cells continued to grow overnight at 37 °C for preparation of large scale growth. Overnight culture was diluted 1:100 into 1 L M9 medium containing 0.5% glycerol, 100 μg/mL ampicillin and trace minerals, cells were grown to an OD_{600} ~ 0.8 and cooled to 18 °C. Selenomethionine (SeMet) was added at a final concentration of 60 μg/mL together with L-isoleucine, L-leucine, L-lysine, L-phenylalanine L-threonine and L-valine to a final concentration of 100 μg/mL and cells were induced with 0.5 mM isopropyl-D-thiogalactopyranoside (IPTG). Cultures were grown overnight at 18°C. The cells were harvested, cell pellets washed and resuspended in 50 mM Tris-HCl (pH 8.0), 500 mM NaCl, 10 mM 2-mercaptoethanol (2-ME), 10% glycerol. Cells were broken in Fast Break reagent (Promega Madison, Wisconsin) supplemented with 10 μg/mL lysozyme and Complete Protease Inhibitor Cocktail (Roche Mannheim, Germany). Cell lysates were centrifuged and the supernatants filtered. A Nickel (II) Sepharose HisTrap column (GE Healthcare Uppsala Sweden) was used for purification of the proteins. Fractions were loaded onto a Hiload 26/60 Superdex200 size exclusion column equilibrated with 20 mM Tris-HCl (pH 7.5) 150 mM NaCl, 2 mM dithiothreitol. Fractions were pooled and concentrated using an Amicon Ultracel 10K centrifugal concentrator. The CdiA-CT•CdiI^{EC3006} and CdiA-CT•CdiI^{Kp342} complexes were concentrated to 12 mg/mL or 10 mg/mL and subsequently incubated overnight on ice with chymotrypsin (20 ng/μL) or trypsin (40 ng/μL). This treatment produced a ~19 kDa fragment of CdiA-CT^{EC3006}, whereas CdiA-CT^{Kp342} was converted into two species of ~14 and ~15 kDa. The digested samples were crystallized directly using the Protein Complex Suite (Qiagen) crystallization screen at 4 °C. CdiA-CT•CdiI ^{EC3006} crystallized from 0.1 M HEPES (pH 7.0), 18% PEG-12,000. CdiA-CT•CdiI^{Kp342} crystal grew in the presence of 0.1 M sodium citrate (pH 5.0), 8% PEG-8000.

Data collection, structure solution and refinement.—Crystals were cryo-protected in reservoir solution supplemented with 17% (CdiA-CT•CdiI^{EC3006}) or 27% (CdiA-CT•CdiI^{Kp342}) glycerol and flash-cooled in liquid nitrogen. Diffraction images were recorded on the ADSC Q315r detector at Structural Biology Center 19-ID beamline at the Advanced Photon Source, Argonne National Laboratory. Single-wavelength anomalous

diffraction (SAD) datasets were collected at 100K near the selenium K-absorption edge to utilize selenium anomalous signal for phasing. Complex crystals diffracted to 2.20 and 2.55 Å for CdiA-CT•CdiI^{EC3006} and CdiA-CT•CdiI^{Kp342}, respectively. The images were processed with the HKL3000 suite (Minor et al., 2006). Intensities were converted to structure factor amplitudes in the Ctruncate program (French and Wilson, 1978; Padilla and Yeates, 2003) from the CCP4 package (Winn et al., 2011). The data collection and processing statistics are given in Table 1.

The structures were solved by the SAD phasing with selenium peak data in the HKL-3000 software pipeline (Minor et al., 2006), utilizing SHELXD, SHELXE (Sheldrick, 2008), MLPHARE (Otwinowski, 1991) and DM (Cowtan, 1994) for heavy atom search and phasing. The initial protein models were built by the HKL builder utilizing Buccaneer (Cowtan, 2006). The final models were obtained through alternating manual rebuilding in Coot (Emsley and Cowtan, 2004) and crystallographic refinement in Refmac (Murshudov et al., 1997; Winn et al., 2011) and Phenix (Adams et al., 2010). In both cases, refinement included optimization of TLS parameters with 37 groups for the CdiA-CT•CdiI^{EC3006} model and 62 groups for CdiA-CT•CdiI^{Kp342}. The CdiA-CT•CdiI^{EC3006} structure contains two copies of the complex, with the following residues most likely present in the crystallized material but not modeled due to the lack of interpretable electron density: Asn174 (chains A and B), Met1 – Asn3 (chain C) and Met1 – Val4 (chain D). The CdiA-CT•CdiI^{Kp342} model contains four copies of the complex, with the following residues missing from the final model: Val139 – Thr143 and Val262 – Lys264 (chain A), Arg116 (chain B), Val139 – 144 and Val262 – Lys264 (chain C), Val139 – Ile142 and Val262 – Lys264 (chain E), Val139 – Asn150 and Asn260 – Arg264 (chain G), and Ile115 – Arg116 (chain H). Refinement statistics are presented in Table 1. The atomic coordinates and structure factors have been deposited in the Protein Data Bank under accession codes 6CP8 (CdiA-CT•CdiI^{EC3006}) and 6CP9 (CdiA-CT•CdiI^{Kp342}). All structure figures were prepared using UCSF Chimera software (Pettersen et al., 2004).

Protein purification for biochemical analyses.—*E. coli* CH2016 cells harboring expression plasmids were cultured at 37 °C with shaking in LB media suppleme nted with 150 μg/mL ampicillin. Cultures were adjusted to 1 mM IPTG at mid-log phase (OD_{600} ~ 0.7) and incubated for an additional 2 h. Cells were harvested by centrifugation and frozen at −80 °C. C ell pellets were re-suspended in lysis buffer [50 mM Tris-HCl (pH 7.5), 150 mM NaCl, 10 mM 2-ME, 0.05% Triton X-100, 20 mM imidazole] and broken by two passages through a French press at 20,000 psi. Cell debris was removed by two rounds of centrifugation at 16,000 ×*g* at 4 °C. His_6-TrxA-EF-Tu (from pCH12603), His_6-TrxA-EF-Ts (from pCH12602) and CdiI-His_6 proteins were purified by Ni^{2+}-affinity chromatography in lysis buffer and eluted with 20 mM Tris-HCl (pH 7.5), 250 mM imidazole. Imidazole was removed by dialysis against 20 mM sodium phosphate (pH 7.8), 150 mM NaCl, 10 mM 2-ME. Native EF-Tu and EF-Ts were cleaved from the fusion proteins with TEV protease, followed by passage over a Ni^{2+}-NTA agarose column to remove the N-terminal His_6-TrxA fragments and TEV protease. Toxins were purified by first isolating the CdiA-CT•CdiI^{Kp342}-His_6 and CdiA-CT•CdiI^{EC3006}-His_6 complexes on Ni^{2+}-NTA agarose as described above. Toxins were eluted with denaturing buffer, 6 M guanidine-HCl in 20 mM Tris-HCl (pH 7.5).

The isolated toxins were then refolded by dialysis against 20 mM sodium phosphate (pH 7.8), 150 mM NaCl, 10 mM 2-ME. Purified proteins were quantified by absorbance at 280 nm using the following extinction coefficients: CdiA-CT^{Kp342}, 13,075 cm^{-1} M^{-1}; CdiI^{Kp342}-His_6, 11,460 cm^{-1} M^{-1}; CdiA-CT^{EC3006}, 23,505 cm^{-1} M^{-1}, CdiI^{EC3006}-His_6, 21,890 cm^{-1} M^{-1}; EF-Tu, 20,400 cm^{-1} M^{-1} and EF-Ts, 4,470 cm^{-1} M^{-1}

In vivo toxin activity and competition co-cultures.—*E. coli* X90 cells carrying plasmids pCH12158 (CdiA-CT•CdiI^{Kp342}-DAS) and pCH12599 (CdiA-CT•CdiI^{EC3006}-DAS) were grown in tetracycline-supplemented LB media for 1 h (OD_{600} ~ 0.1), then expression was induced with 0.4% L-arabinose. Induced cultures were incubated at 37 °C with shaking for 3 h, harve sted into an equal volume of ice-cold methanol and cell pellets frozen at −80 °C prior to RNA extracti on.

E. coli EPI100 inhibitor strains that deliver CdiA-CT^{Kp342} and CdiA-CT^{EC3006} derivatives were mixed with at a 1:1 ratio with rifampicin-resistant *E. coli* MC4100 target cells that harbor empty vector plasmid pTrc99A (*cdiI*$^-$) pCH12865 (*cdiI*^{Kp342}) or pCH11526 (*cdiI*^{EC3006}) in shaking LB media without antibiotics. Viable inhibitor and target bacteria were enumerated (as colony forming units (cfu) per mL on selective media) upon initial mixing and after 1 h of co-culture. Target cell fitness is expressed as the competitive index, which is calculated as the final ratio of target to inhibitor cells divided by the initial ratio at $t = 0$. Competitive indices from three independent experiments are reported together with the average ± standard error of the mean. For the analysis of toxic tRNase activity, samples were harvested into an equal volume of ice-cold methanol after 30 min of co-culture. Cells were collected by centrifugation and frozen at −80 °C for subsequent RNA extraction.

SDS-PAGE and immunoblot analysis.—*E. coli* EPI100 cells carrying chimeric CDI expression plasmids were diluted to OD_{600} ~ 0.05 in LB medium supplemented with Amp and cultured with shaking at 37 °C. Once in mid-log phase, cultures were treated with Spc for 20 min to block protein synthesis. Cells were harvested by centrifugation and frozen at −80 °C. F rozen cell pellets were re-suspended in urea-lysis buffer [50% urea, 150 mM NaCl, 20 mM Tris-HCl (pH 8.0)] and subjected a freeze-thaw cycle to extract proteins for SDS-PAGE and immunoblotting. Urea-soluble protein samples (5 μL) were analyzed by SDS-PAGE on Tris-tricine 6% polyacrylamide gels run at 100 V (constant) for 3 h. Gels were soaked for 15 min in 25 mM Tris, 192 mM glycine (pH 8.6), 10% methanol, then electroblotted to low-fluorescence PVDF membranes using a semi-dry transfer apparatus at 17 V (constant) for 1 h. Membranes were blocked with 4% non-fat milk in PBS for 1 h at room temperature, and incubated with primary antibodies in 0.1% non-fat milk, PBS overnight at 4 °C. Rabbit polyclonal antisera to the N-terminal TPS domain was used at a 1:10,000 dilution (Ruhe et al., 2015). Blots were incubated with 800CW-conjugated goat anti-rabbit IgG (1:40,000 dilution, LICOR) in 0.1% non-fat milk in PBS. Immunoblots were visualized with a LI-COR Odyssey infrared imager.

RNA isolation and analyses.—Frozen cell pellets were resuspended in guanidinium isothiocyanate (GITC)-phenol and total RNA extracted as described (Garza-Sánchez et al., 2006). RNAs (5 μg) were run on 50% urea/7.5% polyacrylamide gels buffered with 0.5× Tris-borate EDTA and electroblotted to positively charged nylon membranes for Northern

blot analysis. Charged and deacylated tRNAs were resolved on 50% urea/10% polyacrylamide gels buffered with 100 mM sodium acetate (pH 5.5) as described (Janssen and Hayes, 2009). Blots were hybridized with [^{32}P]-labeled oligonucleotide probes specific for *E. coli* $tRNA_{GAU}^{Ile}$ (CH577), $tRNA_{UAC}^{Val}$ (CH1248), $tRNA_{UUC}^{Glu}$ (CH1417), $tRNA_{UAA}^{Leu}$ (CH2036) and $tRNA_{GUA}^{Tyr}$ (CH798) (Table S3) and visualized by phosphorimaging using Bio-Rad Quantity One software. S1 nuclease protection analysis was performed as described (Hayes and Sauer, 2003) to map cleavage sites at the 3′-end of $tRNA_{GAU}^{Ile}$. The S1 probe (CH3931) and marker oligonucleotides (CH3932, CH3933 and CH3934) were first radiolabeled at their 3′-termini with [α-^{32}P]-cordycepin triphosphate (Perkin Elmer) and terminal transferase. Labeled oligonucleotides were then passed over a G-25 spin column and treated with unlabeled ATP and T4 polynucleotide kinase to phosphorylate the 5′-termini. The radiolabeled probe was hybridized with RNA samples for 4 h at 50 °C. Hybridization reactions were digested with S1 n uclease at 37 °C for 30 min, then quenched with sodium acetate (pH 5.0) and precipitated with 90% ethanol. The S1 nuclease reactions were run on 50% urea/10% polyacrylamide gels buffered with 0.5× Tris-borate-EDTA and visualized on a Bio-Rad phosphorimager using Quantity One software.

In vitro* nuclease assays.—In vitro* nuclease assays were performed in reaction buffer [20 mM Tris-HCl (pH 7.5), 100 mM NaCl, 5 mM $MgCl_2$, 10 mM 2-ME and 100 μg/μL bovine serum albumin] with toxins used at 1 μM final concentration. Where indicated, purified EF-Tu (1 μM) and EF-Ts (1 μM) were included, and these reactions were supplemented with 1 mM GTP. Immunity proteins were used at 3 μM final concentration. Protein mixtures were equilibrated for 30 min at room temperature. Reactions were then initiated by addition of *E. coli* total RNA to final concentration of 800 ng/μL, followed by incubation for 1 h at 37 °C. Substrate tRNAs were d eacylated at pH 8.9 for 1 h at 37 °C. Reactions were quenched with an equal volume of 2× SDS-urea gel loading buffer and run on 50% urea, 7.5% polyacrylamide gels buffered with 0.5× Tris-borate-EDTA. Gels were electroblotted to nylon membranes for hybridization with radiolabeled oligonucleotide probes as described above.

Quantification and statistical analysis

All competition co-cultures were performed as three independent experiments on separate days. Competitive indices are reported as the average ± SEM as outlined in the figure legends and Method Details.

Data and software availability

Structure datasets generated during this study are available in the Protein Data Bank under accession numbers 6CP8 (http://www.rcsb.org/structure/6CP8) and 6CP9 (http://www.rcsb.org/structure/6CP9).

Supplementary Material

Refer to Web version on PubMed Central for supplementary material.

Acknowledgments

This work was supported by National Institutes of Health grants GM117373 (C.W.G & C.S.H.), GM102318 (C.W.G., C.S.H. & subcontract to A.J.), GM094585 (A.J.), GM115586 (A.J.) and the U. S. Department of Energy, Office of Biological and Environmental Research, under contract DE-AC02-06CH11357 (A.J.).

References

Adams PD, Afonine PV, Bunkoczi G, Chen VB, Davis IW, Echols N, Headd JJ, Hung LW, Kapral GJ, Grosse-Kunstleve RW, et al. (2010). PHENIX: a comprehensive Python-based system for macromolecular structure solution. Acta Crystallogr D Biol Crystallogr 66, 213–221. [PubMed: 20124702]

Aiyar A, Xiang Y, and Leis J (1996). Site-directed mutagenesis using overlap extension PCR. Methods Mol Biol 57, 177–191. [PubMed: 8850005]

Anderson MS, Garcia EC, and Cotter PA (2012). The *Burkholderia bcpAIOB* genes define unique classes of two-partner secretion and contact dependent growth inhibition systems. PLoS Genet 8, e1002877. [PubMed: 22912595]

Anderson MS, Garcia EC, and Cotter PA (2014). Kind discrimination and competitive exclusion mediated by contact-dependent growth inhibition systems shape biofilm community structure. PLoS Pathog 10, e1004076. [PubMed: 24743836]

Aoki SK, Diner EJ, de Roodenbeke CT, Burgess BR, Poole SJ, Braaten BA, Jones AM, Webb JS, Hayes CS, Cotter PA, et al. (2010). A widespread family of polymorphic contact-dependent toxin delivery systems in bacteria. Nature 468, 439–442. [PubMed: 21085179]

Aoki SK, Pamma R, Hernday AD, Bickham JE, Braaten BA, and Low DA (2005). Contact-dependent inhibition of growth in *Escherichia coli*. Science 309, 1245–1248. [PubMed: 16109881]

Aoki SK, Webb JS, Braaten BA, and Low DA (2009). Contact-dependent growth inhibition causes reversible metabolic downregulation in *Escherichia coli*. Journal of bacteriology 191, 1777–1786. [PubMed: 19124575]

Arenas J, Schipper K, van Ulsen P, van der Ende A, and Tommassen J (2013). Domain exchange at the 3′ end of the gene encoding the fratricide meningococcal two-partner secretion protein A. BMC Genomics 14, 622. [PubMed: 24034852]

Batot G, Michalska K, Ekberg G, Irimpan EM, Joachimiak G, Jedrzejczak R, Babnigg G, Hayes CS, Joachimiak A, and Goulding CW (2017). The CDI toxin of Yersinia kristensenii is a novel bacterial member of the RNase A superfamily. Nucleic Acids Res 45, 5013–5025. [PubMed: 28398546]

Beck CM, Morse RP, Cunningham DA, Iniguez A, Low DA, Goulding CW, and Hayes CS (2014). CdiA from *Enterobacter cloacae* delivers a toxic ribosomal RNase into target bacteria. Structure 22, 707–718. [PubMed: 24657090]

Betat H, Rammelt C, and Morl M (2010). tRNA nucleotidyltransferases: ancient catalysts with an unusual mechanism of polymerization. Cell Mol Life Sci 67, 1447–1463. [PubMed: 20155482]

Cao Z, Casabona MG, Kneuper H, Chalmers JD, and Palmer T (2016). The type VII secretion system of Staphylococcus aureus secretes a nuclease toxin that targets competitor bacteria. Nat Microbiol 2, 16183. [PubMed: 27723728]

Cascales E, Buchanan SK, Duche D, Kleanthous C, Lloubes R, Postle K, Riley M, Slatin S, and Cavard D (2007). Colicin biology. Microbiol. Mol. Biol. Rev 71, 158–229. [PubMed: 17347522]

Cowtan K (1994). DM: an automated procedure for phase improvement by density modification. Joint CCP4 and ESF-EACBM newsletter on protein crystallography 31, 34–38.

Cowtan K (2006). The Buccaneer software for automated model building. 1. Tracing protein chains. Acta Crystallogr D Biol Crystallogr 62, 1002–1011. [PubMed: 16929101]

Cruz JW, Sharp JD, Hoffer ED, Maehigashi T, Vvedenskaya IO, Konkimalla A, Husson RN, Nickels BE, Dunham CM, and Woychik NA (2015). Growth-regulating Mycobacterium tuberculosis VapC-mt4 toxin is an isoacceptor-specific tRNase. Nat Commun 6, 7480. [PubMed: 26158745]

Davis IW, Murray LW, Richardson JS, and Richardson DC (2004). MOLPROBITY: structure validation and all-atom contact analysis for nucleic acids and their complexes. Nucleic Acids Res 32, W615–619. [PubMed: 15215462]

Diner EJ, Beck CM, Webb JS, Low DA, and Hayes CS (2012). Identification of a target cell permissive factor required for contact-dependent growth inhibition (CDI). Genes Dev 26, 515–525. [PubMed: 22333533]

Dunican BF, Hiller DA, and Strobel SA (2015). Transition State Charge Stabilization and Acid-Base Catalysis of mRNA Cleavage by the Endoribonuclease RelE. Biochemistry 54, 7048–7057. [PubMed: 26535789]

Emsley P, and Cowtan K (2004). Coot: model-building tools for molecular graphics. Acta Crystallogr D Biol Crystallogr 60, 2126–2132. [PubMed: 15572765]

Eschenfeldt WH, Lucy S, Millard CS, Joachimiak A, and Mark ID (2009). A family of LIC vectors for high-throughput cloning and purification of proteins. Methods Mol Biol 498, 105–115. [PubMed: 18988021]

Eschenfeldt WH, Makowska-Grzyska M, Stols L, Donnelly MI, Jedrzejczak R, and Joachimiak A (2013). New LIC vectors for production of proteins from genes containing rare codons. J Struct Funct Genomics 14, 135–144. [PubMed: 24057978]

French S, and Wilson K (1978). On the treatment of negative intensity observations. Acta Crystallogr A A34, 517–525.

Garcia-Bayona L, Guo MS, and Laub MT (2017). Contact-dependent killing by Caulobacter crescentus via cell surface-associated, glycine zipper proteins. Elife 6.

Garza-Sánchez F, Janssen BD, and Hayes CS (2006). Prolyl-tRNA(Pro) in the A-site of SecM-arrested ribosomes inhibits the recruitment of transfer-messenger RNA. J Biol Chem 281, 34258–34268. [PubMed: 16968693]

Gerdes K, and Maisonneuve E (2012). Bacterial persistence and toxin-antitoxin loci. Annu Rev Microbiol 66, 103–123. [PubMed: 22994490]

Graille M, Mora L, Buckingham RH, van Tilbeurgh H, and de Zamaroczy M (2004). Structural inhibition of the colicin D tRNase by the tRNA-mimicking immunity protein. EMBO J 23, 1474–1482. [PubMed: 15014439]

Griffin MA, Davis JH, and Strobel SA (2013). Bacterial toxin RelE: a highly efficient ribonuclease with exquisite substrate specificity using atypical catalytic residues. Biochemistry 52, 8633–8642. [PubMed: 24251350]

Hachani A, Allsopp LP, Oduko Y, and Filloux A (2014). The VgrG proteins are "a la carte" delivery systems for bacterial type VI effectors. J Biol Chem 289, 17872–17884. [PubMed: 24794869]

Hayes CS, and Sauer RT (2003). Cleavage of the A site mRNA codon during ribosome pausing provides a mechanism for translational quality control. Mol. Cell 12, 903–911. [PubMed: 14580341]

Holberger LE, Garza-Sanchez F, Lamoureux J, Low DA, and Hayes CS (2012). A novel family of toxin/antitoxin proteins in Bacillus species. FEBS Lett 586, 132–136. [PubMed: 22200572]

Holm L, and Rosenstrom P (2010). Dali server: conservation mapping in 3D. Nucleic Acids Res 38, W545–549. [PubMed: 20457744]

Hood RD, Singh P, Hsu F, Guvener T, Carl MA, Trinidad RR, Silverman JM, Ohlson BB, Hicks KG, Plemel RL, et al. (2010). A type VI secretion system of *Pseudomonas aeruginosa* targets a toxin to bacteria. Cell Host Microbe 7, 25–37. [PubMed: 20114026]

Jamet A, Jousset AB, Euphrasie D, Mukorako P, Boucharlat A, Ducousso A, Charbit A, and Nassif X (2015). A new family of secreted toxins in pathogenic *Neisseria* species. PLoS Pathog 11, e1004592. [PubMed: 25569427]

Janiak F, Dell VA, Abrahamson JK, Watson BS, Miller DL, and Johnson AE (1990). Fluorescence characterization of the interaction of various transfer RNA species with elongation factor Tu.GTP: evidence for a new functional role for elongation factor Tu in protein biosynthesis. Biochemistry 29, 4268–4277. [PubMed: 2190631]

Janssen BD, and Hayes CS (2009). Kinetics of paused ribosome recycling in Escherichia coli. J Mol Biol 394, 251–267. [PubMed: 19761774]

Johnson PM, Beck CM, Morse RP, Garza-Sanchez F, Low DA, Hayes CS, and Goulding CW (2016a). Unraveling the essential role of CysK in CDI toxin activation. Proc Natl Acad Sci U S A 113, 9792–9797. [PubMed: 27531961]

Johnson PM, Gucinski GC, Garza-Sanchez F, Wong T, Hung LW, Hayes CS, and Goulding CW (2016b). Functional Diversity of Cytotoxic tRNase/Immunity Protein Complexes from *Burkholderia pseudomallei*. J Biol Chem 291, 19387–19400. [PubMed: 27445337]

Jones AM, Garza-Sanchez F, So J, Hayes CS, and Low DA (2017). Activation of contact-dependent antibacterial tRNase toxins by translation elongation factors. Proc Natl Acad Sci U S A 114, E1951–E1957. [PubMed: 28223500]

Karplus PA, and Diederichs K (2012). Linking crystallographic model and data quality. Science 336, 1030–1033. [PubMed: 22628654]

Koskiniemi S, Lamoureux JG, Nikolakakis KC, t'Kint de Roodenbeke C, Kaplan MD, Low DA, and Hayes CS (2013). Rhs proteins from diverse bacteria mediate intercellular competition. Proc Natl Acad Sci U S A 110, 7032–7037. [PubMed: 23572593]

Levitz R, Chapman D, Amitsur M, Green R, Snyder L, and Kaufmann G (1990). The optional E. coli prr locus encodes a latent form of phage T4-induced anticodon nuclease. EMBO J 9, 1383–1389. [PubMed: 1691706]

MacIntyre DL, Miyata ST, Kitaoka M, and Pukatzki S (2010). The *Vibrio cholerae* type VI secretion system displays antimicrobial properties. Proc Natl Acad Sci U S A 107, 19520–19524. [PubMed: 20974937]

McGinness KE, Baker TA, and Sauer RT (2006). Engineering controllable protein degradation. Mol. Cell 22, 701–707. [PubMed: 16762842]

Michalska K, Gucinski GC, Garza-Sanchez F, Johnson PM, Stols LM, Eschenfeldt WH, Babnigg G, Low DA, Goulding CW, Joachimiak A, et al. (2017). Structure of a novel antibacterial toxin that exploits elongation factor Tu to cleave specific transfer RNAs. Nucleic Acids Res 45, 10306–10320. [PubMed: 28973472]

Michalska K, Quan Nhan D, Willett JLE, Stols LM, Eschenfeldt WH, Jones AM, Nguyen JY, Koskiniemi S, Low DA, Goulding CW, et al. (2018). Functional plasticity of antibacterial EndoU toxins. Mol Microbiol 109, 509–527. [PubMed: 29923643]

Minor W, Cymborowski M, Otwinowski Z, and Chruszcz M (2006). HKL-3000: the integration of data reduction and structure solution--from diffraction images to an initial model in minutes. Acta Crystallogr D Biol Crystallogr 62, 859–866. [PubMed: 16855301]

Morse RP, Nikolakakis KC, Willett JL, Gerrick E, Low DA, Hayes CS, and Goulding CW (2012). Structural basis of toxicity and immunity in contact-dependent growth inhibition (CDI) systems. Proc Natl Acad Sci U S A 109, 21480–21485. [PubMed: 23236156]

Morse RP, Willett JL, Johnson PM, Zheng J, Credali A, Iniguez A, Nowick JS, Hayes CS, and Goulding CW (2015). Diversification of beta-Augmentation Interactions between CDI Toxin/Immunity Proteins. J Mol Biol 427, 3766–3784. [PubMed: 26449640]

Murshudov GN, Vagin AA, and Dodson EJ (1997). Refinement of macromolecular structures by the maximum-likelihood method. Acta Crystallogr D Biol Crystallogr 53, 240–255. [PubMed: 15299926]

Neubauer C, Gao YG, Andersen KR, Dunham CM, Kelley AC, Hentschel J, Gerdes K, Ramakrishnan V, and Brodersen DE (2009). The structural basis for mRNA recognition and cleavage by the ribosome-dependent endonuclease RelE. Cell 139, 1084–1095. [PubMed: 20005802]

Nikolakakis K, Amber S, Wilbur JS, Diner EJ, Aoki SK, Poole SJ, Tuanyok A, Keim PS, Peacock S, Hayes CS, et al. (2012). The toxin/immunity network of *Burkholderia pseudomallei* contact-dependent growth inhibition (CDI) systems. Mol Microbiol 84, 516–529. [PubMed: 22435733]

Nissen P, Thirup S, Kjeldgaard M, and Nyborg J (1999). The crystal structure of Cys-tRNACys-EF-Tu-GDPNP reveals general and specific features in the ternary complex and in tRNA. Structure 7, 143–156. [PubMed: 10368282]

Ogawa T, Tomita K, Ueda T, Watanabe K, Uozumi T, and Masaki H (1999). A cytotoxic ribonuclease targeting specific transfer RNA anticodons. Science 283, 2097–2100. [PubMed: 10092236]

Otwinowski Z (1991). Maximum likelihood refinement of heavy atom parameters. In Proceedings of the CCP4 Study Weekend 25–26 January 1991 (Daresbury Laboratory, Warrington, U.K.), pp. 80–85.

Padilla JE, and Yeates TO (2003). A statistic for local intensity differences: robustness to anisotropy and pseudo-centering and utility for detecting twinning. Acta Crystallogr D Biol Crystallogr 59, 1124–1130. [PubMed: 12832754]

Pettersen EF, Goddard TD, Huang CC, Couch GS, Greenblatt DM, Meng EC, and Ferrin TE (2004). UCSF Chimera--a visualization system for exploratory research and analysis. J Comput Chem 25, 1605–1612. [PubMed: 15264254]

Poole SJ, Diner EJ, Aoki SK, Braaten BA, T'Kint de Roodenbeke C, Low DA, and Hayes CS (2011). Identification of functional toxin/immunity genes linked to contact-dependent growth inhibition (CDI) and rearrangement hotspot (Rhs) systems. PLoS Genet. 7, e1002217. [PubMed: 21829394]

Riley MA (1993a). Molecular mechanisms of colicin evolution. Mol Biol Evol 10, 1380–1395. [PubMed: 8277860]

Riley MA (1993b). Positive selection for colicin diversity in bacteria. Mol Biol Evol 10, 1048–1059. [PubMed: 8412648]

Ruhe ZC, Nguyen JY, Chen AJ, Leung NY, Hayes CS, and Low DA (2016). CDI Systems Are Stably Maintained by a Cell-Contact Mediated Surveillance Mechanism. PLoS Genet 12, e1006145. [PubMed: 27355474]

Ruhe ZC, Nguyen JY, Xiong J, Koskiniemi S, Beck CM, Perkins BR, Low DA, and Hayes CS (2017). CdiA Effectors Use Modular Receptor-Binding Domains To Recognize Target Bacteria. MBio 8.

Ruhe ZC, Subramanian P, Song K, Nguyen JY, Stevens TA, Low DA, Jensen GJ, and Hayes CS (2018). Programmed Secretion Arrest and Receptor-Triggered Toxin Export during Antibacterial Contact-Dependent Growth Inhibition. Cell 175, 921–933 e914. [PubMed: 30388452]

Ruhe ZC, Townsley L, Wallace AB, King A, Van der Woude MW, Low DA, Yildiz FH, and Hayes CS (2015). CdiA promotes receptor-independent intercellular adhesion. Mol Microbiol 98, 175–192. [PubMed: 26135212]

Schifano JM, Cruz JW, Vvedenskaya IO, Edifor R, Ouyang M, Husson RN, Nickels BE, and Woychik NA (2016). tRNA is a new target for cleavage by a MazF toxin. Nucleic Acids Res 44, 1256–1270. [PubMed: 26740583]

Sheldrick GM (2008). A short history of SHELX. Acta Crystallogr A 64, 112–122. [PubMed: 18156677]

Shneider MM, Buth SA, Ho BT, Basler M, Mekalanos JJ, and Leiman PG (2013). PAAR-repeat proteins sharpen and diversify the type VI secretion system spike. Nature 500, 350–353. [PubMed: 23925114]

Souza DP, Oka GU, Alvarez-Martinez CE, Bisson-Filho AW, Dunger G, Hobeika L, Cavalcante NS, Alegria MC, Barbosa LR, Salinas RK, et al. (2015). Bacterial killing via a type IV secretion system. Nat Commun 6, 6453. [PubMed: 25743609]

Steczkiewicz K, Muszewska A, Knizewski L, Rychlewski L, and Ginalski K (2012). Sequence, structure and functional diversity of PD-(D/E)XK phosphodiesterase superfamily. Nucleic Acids Res 40, 7016–7045. [PubMed: 22638584]

Thomason L, Court DL, Bubunenko M, Costantino N, Wilson H, Datta S, and Oppenheim A (2007). Recombineering: genetic engineering in bacteria using homologous recombination Current protocols in molecular biology / edited by Ausubel Frederick M. ... [et al. *Chapter 1,* Unit 1 16.

Tomita K, Ogawa T, Uozumi T, Watanabe K, and Masaki H (2000). A cytotoxic ribonuclease which specifically cleaves four isoaccepting arginine tRNAs at their anticodon loops. Proc Natl Acad Sci U S A 97, 8278–8283. [PubMed: 10880568]

Van Melderen L (2010). Toxin-antitoxin systems: why so many, what for? Curr Opin Microbiol 13, 781–785. [PubMed: 21041110]

Walker D, Lancaster L, James R, and Kleanthous C (2004). Identification of the catalytic motif of the microbial ribosome inactivating cytotoxin colicin E3. Protein Sci 13, 1603–1611. [PubMed: 15133158]

Webb JS, Nikolakakis KC, Willett JL, Aoki SK, Hayes CS, and Low DA (2013). Delivery of CdiA nuclease toxins into target cells during contact-dependent growth inhibition. PLoS ONE 8, e57609. [PubMed: 23469034]

Whitney JC, Beck CM, Goo YA, Russell AB, Harding BN, De Leon JA, Cunningham DA, Tran BQ, Low DA, Goodlett DR, et al. (2014). Genetically distinct pathways guide effector export through the type VI secretion system. Mol Microbiol 92, 529–542. [PubMed: 24589350]

Whitney JC, Peterson SB, Kim J, Pazos M, Verster AJ, Radey MC, Kulasekara HD, Ching MQ, Bullen NP, Bryant D, et al. (2017). A broadly distributed toxin family mediates contact-dependent antagonism between gram-positive bacteria. Elife 6.

Willett JL, Gucinski GC, Fatherree JP, Low DA, and Hayes CS (2015a). Contact-dependent growth inhibition toxins exploit multiple independent cell-entry pathways. Proc Natl Acad Sci U S A 112, 11341–11346. [PubMed: 26305955]

Willett JL, Ruhe ZC, Goulding CW, Low DA, and Hayes CS (2015b). Contact-Dependent Growth Inhibition (CDI) and CdiB/CdiA Two-Partner Secretion Proteins. J Mol Biol 427, 3754–3765. [PubMed: 26388411]

Winn MD, Ballard CC, Cowtan KD, Dodson EJ, Emsley P, Evans PR, Keegan RM, Krissinel EB, Leslie AG, McCoy A, et al. (2011). Overview of the CCP4 suite and current developments. Acta Crystallogr D Biol Crystallogr 67, 235–242. [PubMed: 21460441]

Winther K, Tree JJ, Tollervey D, and Gerdes K (2016). VapCs of Mycobacterium tuberculosis cleave RNAs essential for translation. Nucleic Acids Res 44, 9860–9871. [PubMed: 27599842]

Winther KS, and Gerdes K (2011). Enteric virulence associated protein VapC inhibits translation by cleavage of initiator tRNA. Proc Natl Acad Sci U S A 108, 7403–7407. [PubMed: 21502523]

Yajima S, Inoue S, Ogawa T, Nonaka T, Ohsawa K, and Masaki H (2006). Structural basis for sequence-dependent recognition of colicin E5 tRNase by mimicking the mRNA-tRNA interaction. Nucleic Acids Res 34, 6074–6082. [PubMed: 17099236]

Yanagisawa T, Lee JT, Wu HC, and Kawakami M (1994). Relationship of protein structure of isoleucyl-tRNA synthetase with pseudomonic acid resistance of Escherichia coli. A proposed mode of action of pseudomonic acid as an inhibitor of isoleucyl-tRNA synthetase. J Biol Chem 269, 24304–24309. [PubMed: 7929087]

Zhang D, de Souza RF, Anantharaman V, Iyer LM, and Aravind L (2012). Polymorphic toxin systems: Comprehensive characterization of trafficking modes, processing, mechanisms of action, immunity and ecology using comparative genomics. Biol Direct 7, 18. [PubMed: 22731697]

Zhang D, Iyer LM, and Aravind L (2011). A novel immunity system for bacterial nucleic acid degrading toxins and its recruitment in various eukaryotic and DNA viral systems. Nucleic Acids Res 39, 4532–4552. [PubMed: 21306995]

Zhang D, Iyer LM, Burroughs AM, and Aravind L (2014). Resilience of biochemical activity in protein domains in the face of structural divergence. Curr Opin Struct Biol 26, 92–103. [PubMed: 24952217]

Highlights

- The crystal structures of two CDI toxin•immunity protein complexes are presented
- Both toxins are isoacceptor specific ribonucleases that cleave deacylated $tRNA_{GAU}^{Ile}$
- The immunity proteins do not share any sequence or structural homology
- Similarities between these tRNase toxins likely arose through convergent evolution

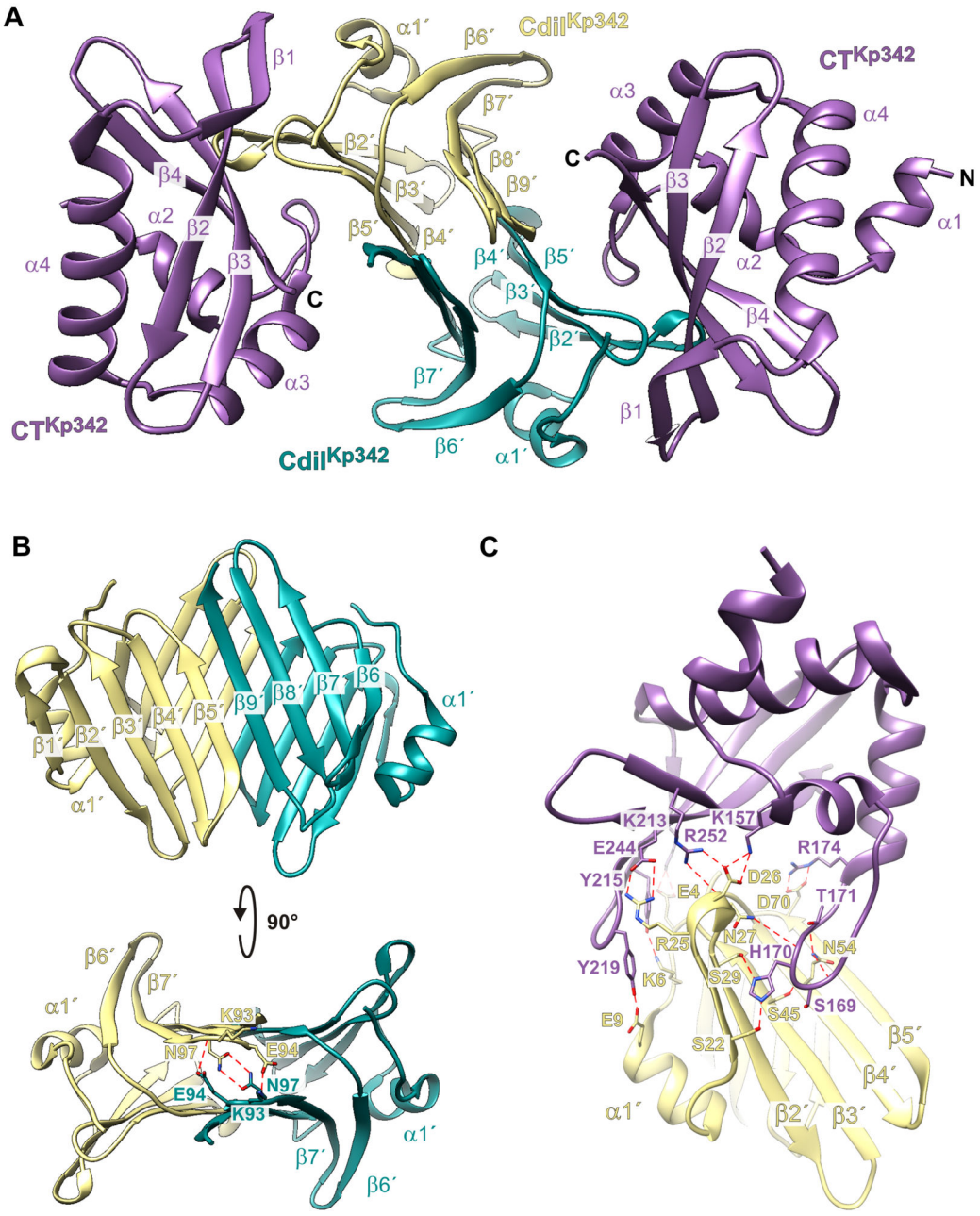

Figure 1. Structure of the CdiA-CT•CdiI^{Kp342} complex.

A) Secondary structure elements of the CdiA-CT•CdiI^{Kp342} complex. **B**) CdiI^{Kp342} forms a dimeric -sandwich. **C**) Direct H-bond and ion-pair contacts. See also Figures S1 and S2.

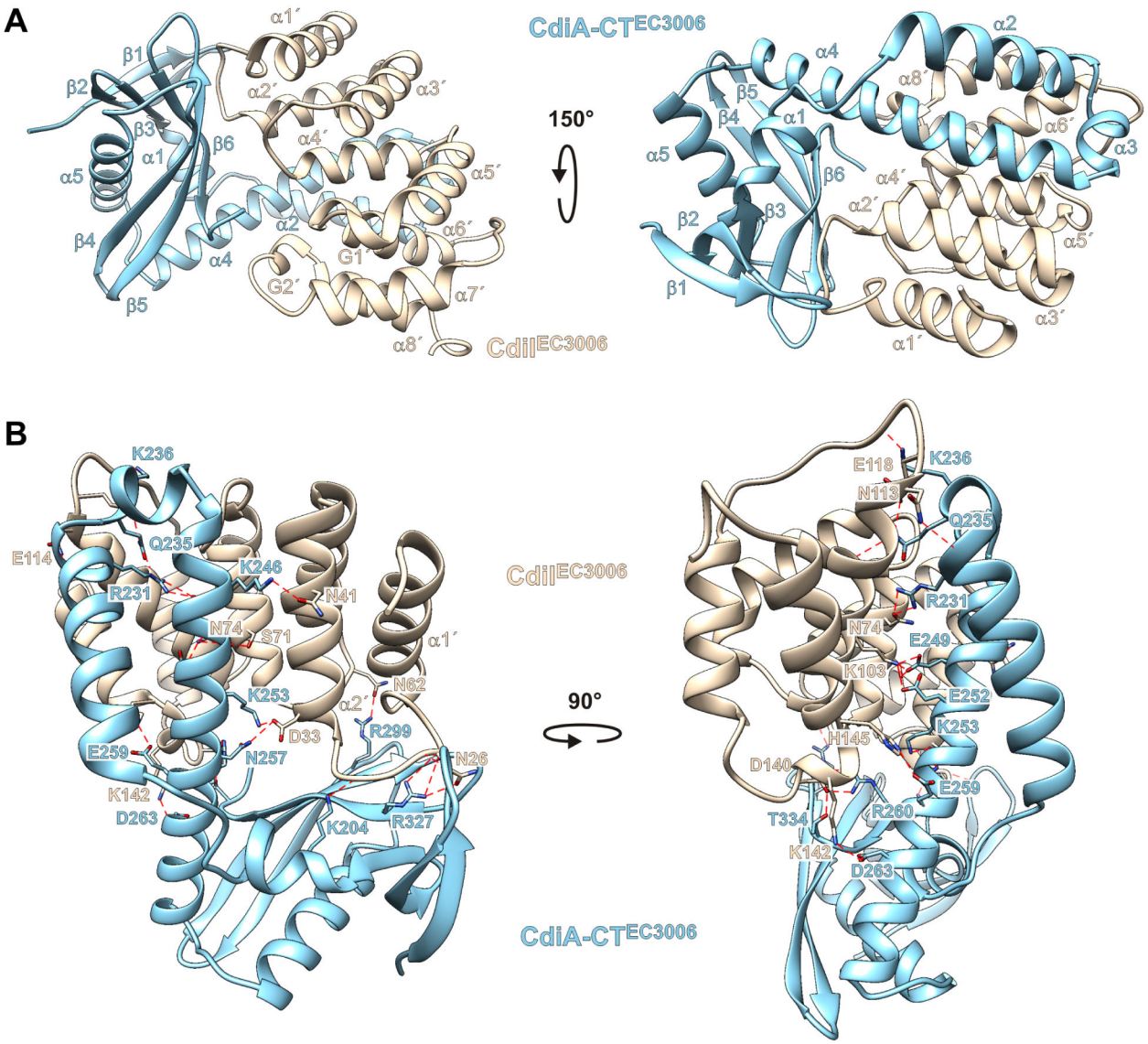

Figure 2. Structure of the CdiA-CT•CdiI^{EC3006} complex.

A) Secondary structure elements of the CdiA-CT•CdiI^{EC3006} complex. **B**) Direct H-bond and ion-pair contacts. See also Figures S1 and S3.

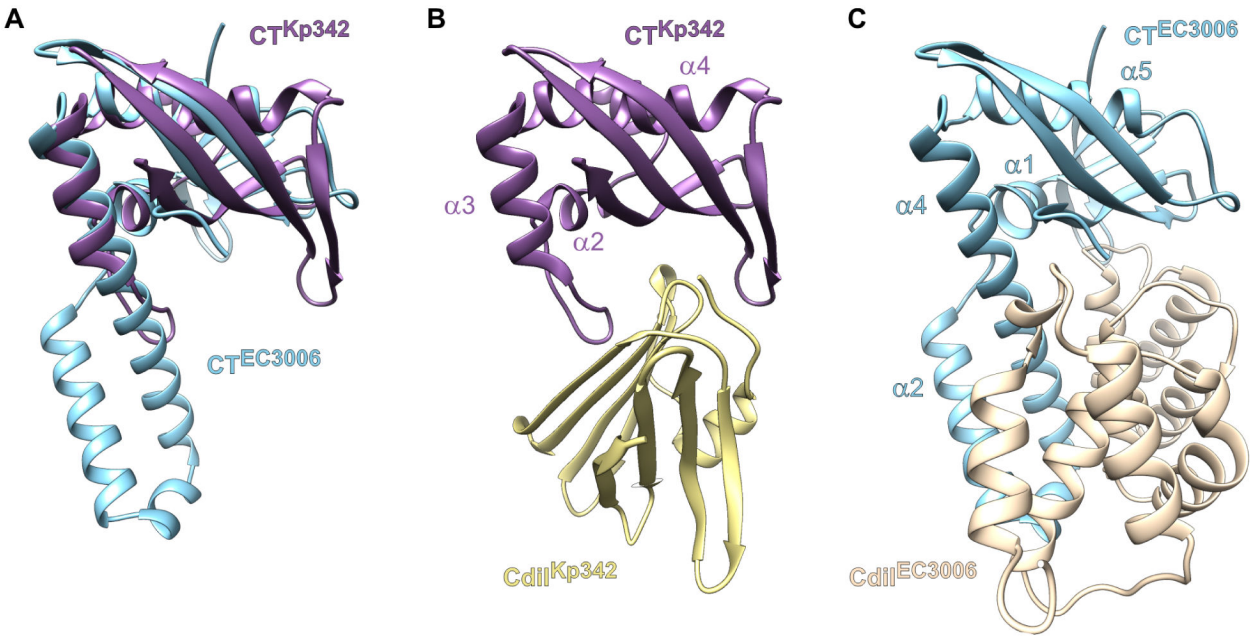

Figure 3. CdiA-CT^{Kp342} and CdiA-CT^{EC3006} are structurally similar.

A) Superimposition of the CdiA-CT^{Kp342} and CdiA-CT^{EC3006} toxin domains. See also Table S2. **B**) Binding position of the CdiI^{Kp342} immunity protein. **C**) Binding position of the CdiI^{EC3006} immunity protein.

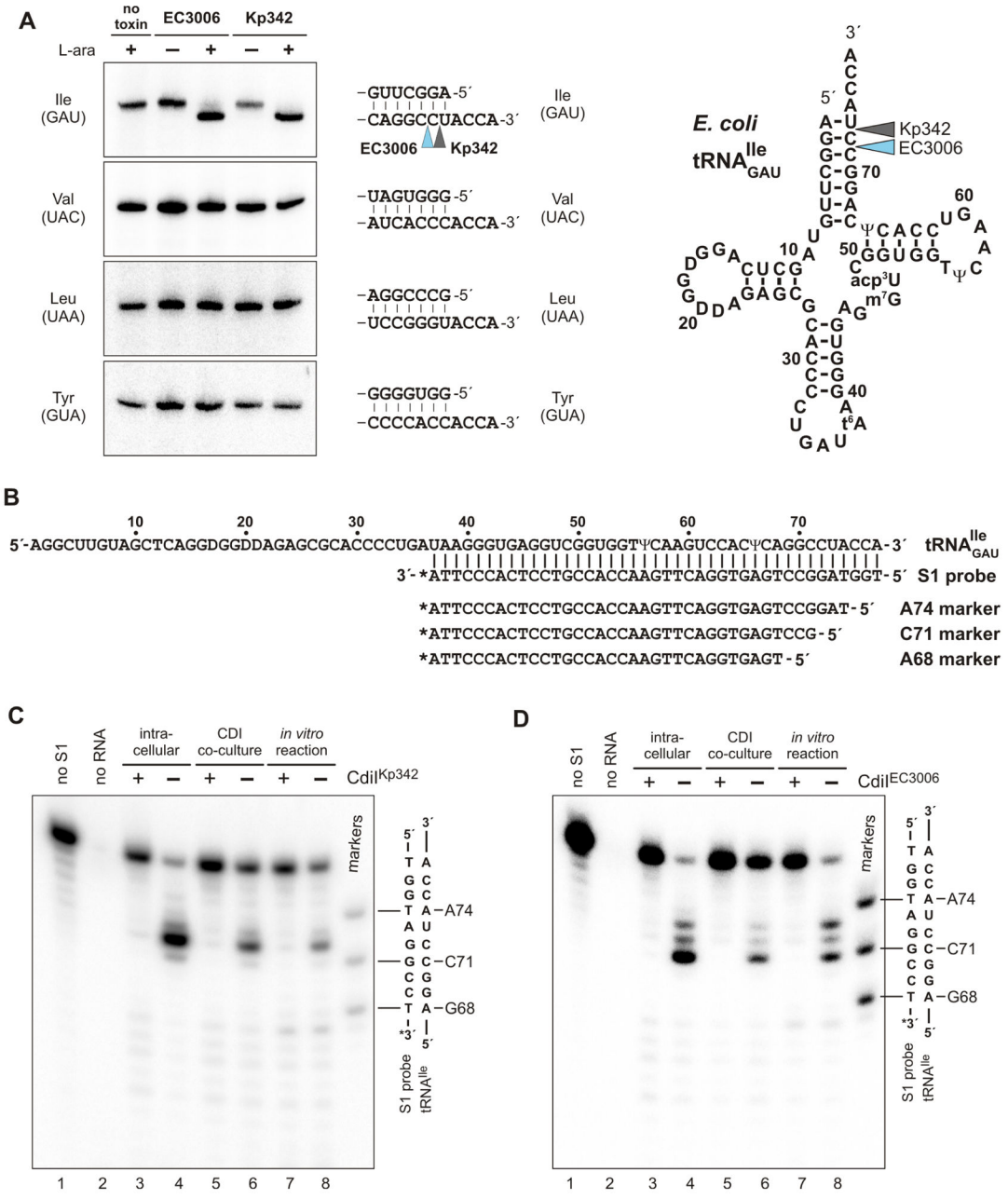

Figure 4. CdiA-CT^{EC3006} and CdiA-CT^{Kp342} cleave tRNA$_{GAU}^{Ile}$.

A) Toxin activation inside *E. coli* cells leads to tRNA$_{GAU}^{Ile}$ cleavage. Toxin expression was induced L-arabinose where indicated and RNA isolated for Northern blot hybridization using probes to the indicated tRNAs. Aminoacyl acceptor stem sequences and toxin cleavage sites are indicated on the right. **B**) tRNA$_{GAU}^{Ile}$ sequence showing the hybridized S1 probe and oligonucleotide standards used to map toxin cleavage sites. **C**) S1 protection analysis of tRNA$_{GAU}^{Ile}$ cleaved by CdiA-CT^{Kp342}. RNA samples were isolated from i) cells intoxicated by intracellular CdiA-CT^{Kp342} expression, ii) competition co-cultures and iii) *in vitro* nuclease reactions. Where indicated, the neutralizing effect of CdiI^{Kp342} was examined. Samples were hybridized with 3′-radiolabeled S1 probe and treated with S1

nuclease as described in Methods. A portion of the S1 probe-$tRNA_{GAU}^{Ile}$ heteroduplex sequence is shown to the right of the autoradiogram. **D**) S1 protection analysis of $tRNA_{GAU}^{Ile}$ cleaved by CdiA-CT^{EC3006}. Samples were analyzed as described for panel C.

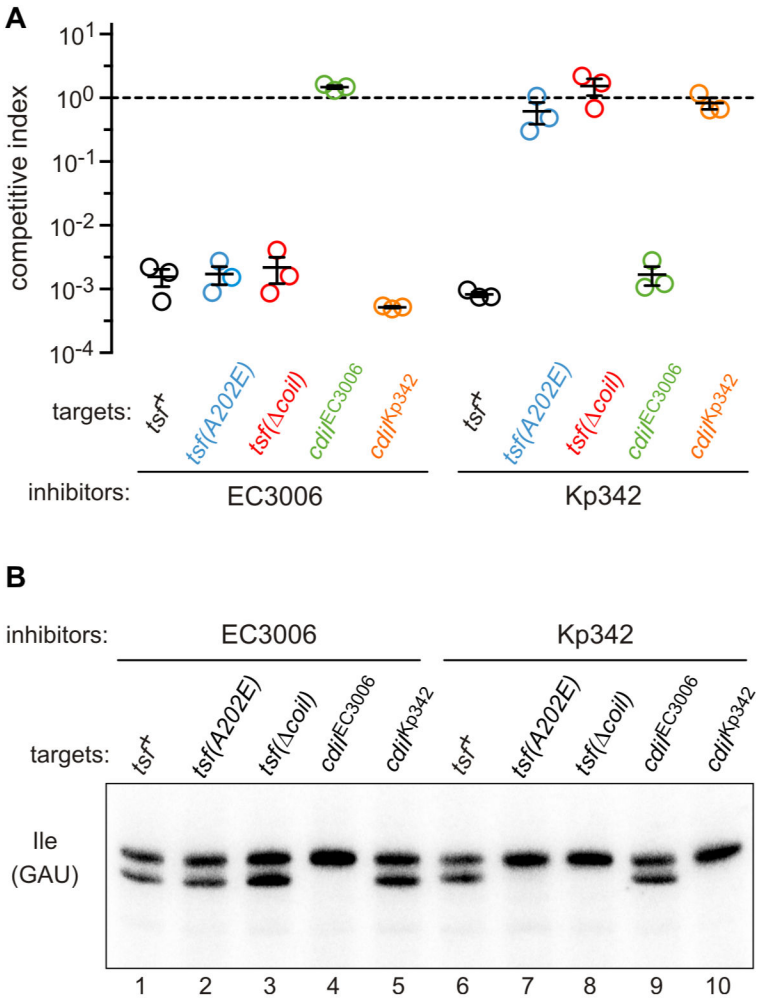

Figure 5. *tsf* mutants are resistant to CdiA-CT^{Kp342}, but not CdiA-CT^{EC3006} intoxication.

A) Competition co-cultures. Target bacteria were co-cultured at a 1:1 ratio with inhibitor cells that deliver either CdiA-CT^{EC3006} or CdiA-CT^{Kp342}. Competitive index is the ratio of viable target to inhibitor cells at 1 h divided by the initial ratio. Data are from three independent experiments together with the average ± SEM. **B**) Toxin activity in co-cultures. Inhibitor strains were co-cultured with the indicated target cells for 30 min, then RNA was isolated for Northern blot analysis of $tRNA_{GAU}^{Ile}$.

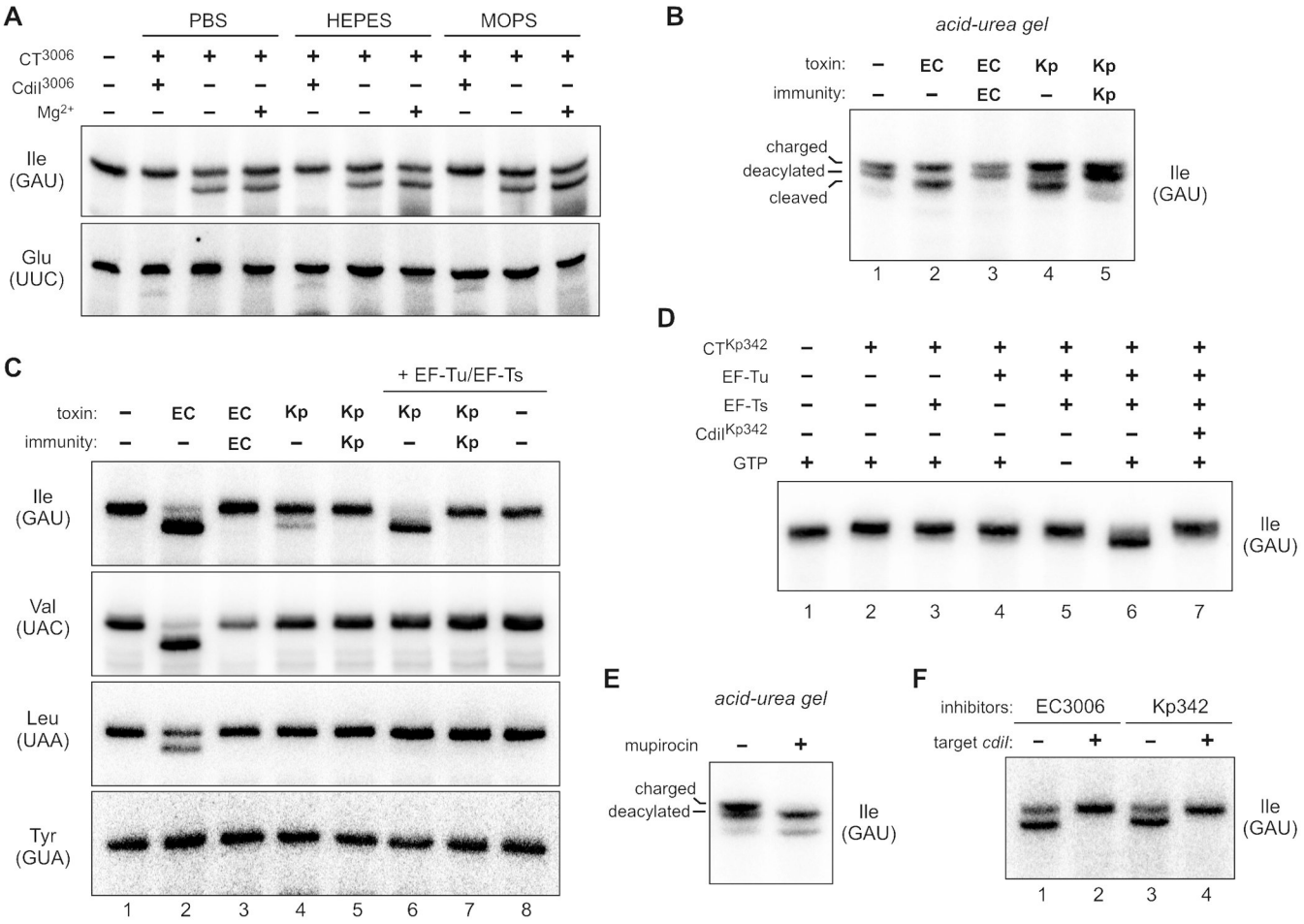

Figure 6. CdiA-CT^{Kp342} and CdiA-CT^{C3006} are specific for deacylated tRNA$_{GAU}^{Ile}$.

A) *In vitro* nuclease reactions. Total RNA isolated from *E. coli* was incubated with purified CdiA-CT^{EC3006} and analyzed by Northern blotting as described in Methods. Where indicated, reactions were supplemented with CdiI^{EC3006} or 5 mM $MgCl_2$. **B**) Acid-urea gel analysis of nuclease reactions. **C**) *In vitro* nuclease assays using deacylated tRNA. Where indicated, purified EF-Tu and EF-Ts were included in the reactions. **D**) CdiA-CT^{Kp342} requires EF-Tu, EF-Ts and GTP to support tRNase activity. Deacylated tRNA was treated with the indicated proteins and tRNA$_{GAU}^{Ile}$ analyzed by Northern blotting. **E**) Acid-urea gel analysis of tRNA$_{GAU}^{Ile}$ isolated from mupirocin-treated cells. **F**) Northern blot analysis of tRNA$_{GAU}^{Ile}$ isolated from competition co-cultures in the presence of mupirocin.

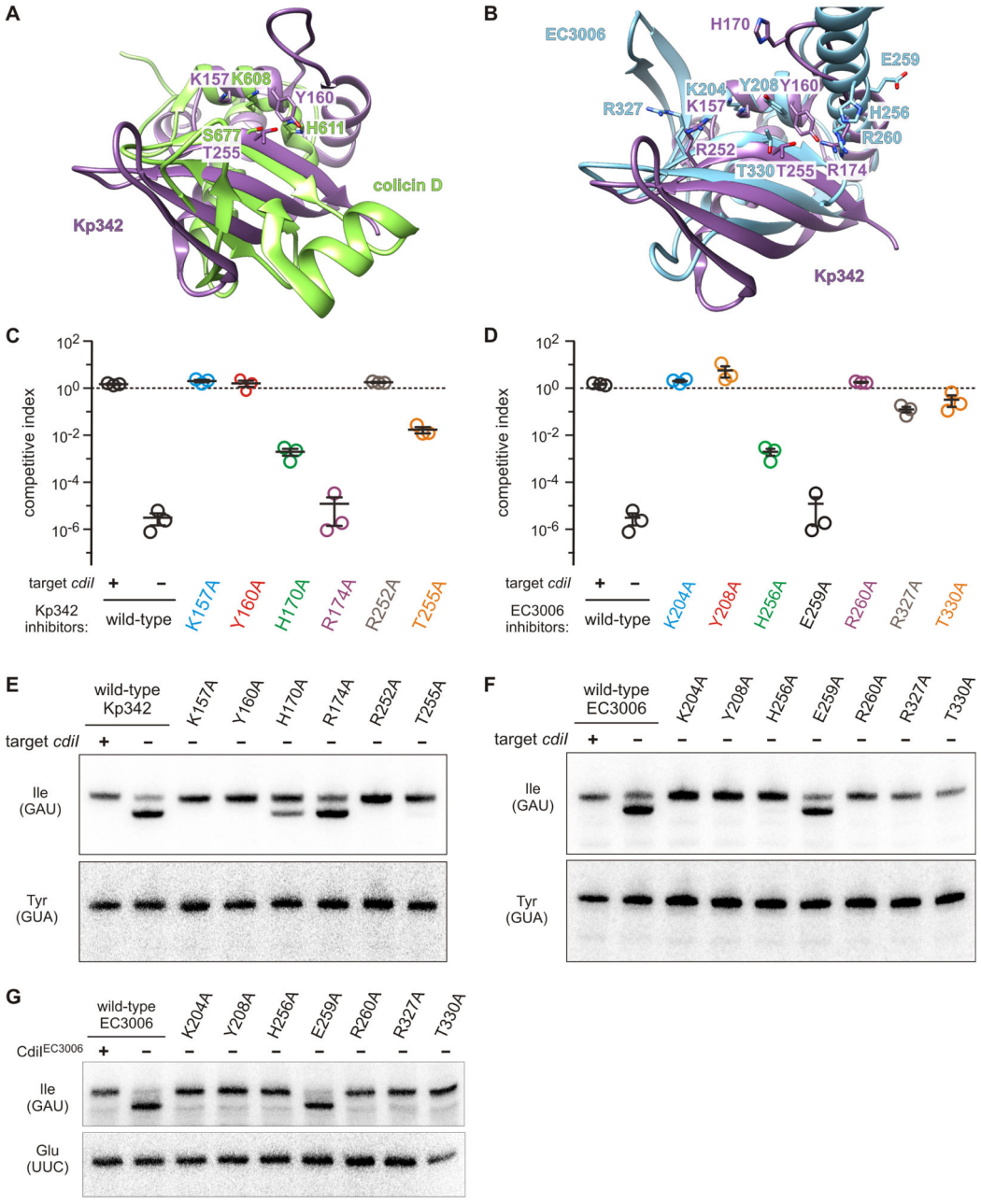

Figure 7. The nuclease active sites of CdiA-CT^{Kp342} and CdiA-CT^{EC3006}.

A) Superimposition of CdiA-CT^{Kp342} onto the nuclease domain of colicin D. **B**) Putative active sites of CdiA-CT^{Kp342} and CdiA-CT^{EC3006} nuclease domains. **C** & **D**) Competition co-cultures. Target bacteria were co-cultured at a 1:1 ratio with inhibitor cells that deliver the indicated CdiA-CT^{Kp342} (panel **C**) or CdiA-CT^{EC3006} (panel **D**) variants. Competitive indices are calculated as the ratio of viable target to inhibitor cells at 1 h divided by the initial ratio. Data are from three independent experiments together with the average ± SEM. See also Figure S4. **E** & **F**) Toxin activities in co-cultures. Inhibitor strains were co-cultured with the indicated target cells for 30 min, then total RNA was isolated for Northern blot

analysis. **G**) *In vitro* nuclease activity of CdiA-CT^{EC3006} variants. The indicated CdiA-CT^{EC3006} domains were purified and incubated with deacylated tRNA substrate.

Table 1.

Data processing and refinement statistics.

Data processing		
Protein	**CdiA-CT•CdiI^{EC3006}**	**CdiA-CT•CdiI^{Kp342}**
Wavelength (Å)	0.9792	0.9792
Resolution range (Å)[a]	30.0 - 2.20 (2.24 - 2.20)	30.0 - 2.55 (2.59 - 2.55)
Space group	$P2_1$	$P2_12_12$
Unit cell parameters (Å, °)	50.71 106.53 72.65 101.0	102.64 145.45 84.28
Unique reflections	38,085 (1,879)	41,852 (2,053)
Multiplicity	4.2 (3.8)	25.6 (22.7)
Completeness (%)	99.9 (100)	99.9 (100)
<I >/< σI>	11.28 (1.96)	34.5 (1.8)
R_{merge}[b]	0.127 (0.749)	0.144 (2.27)
CC1/2[c]	0.664	0.722
CC*[c]	0.893	0.916
Refinement		
Resolution (Å)	30.0 - 2.20	30.0 - 2.55
Reflections work/test set	36,865/1,189	39,752/2,035
R_{work}/ R_{free}[d]	0.176/0.218	0.181/0.232
Average B factor (Å^2) (No of atoms)		
macromolecule	40.6 (5,010)	88.0 (7,377)
ligands	51.6 (27)	
solvent	40.6 (174)	77.6 (23)
Rmsd bond lengths (Å)	0.011	0.008
Rmsd bond angles (°)	1.06	0.965
Ramachandran favored[e] (%)	98.1	99.2
Ramachandran outliers	0	0
Clashscore[e]	3.51	5.8
PDB ID	**6CP8**	**6CP9**

[a] Values in parentheses correspond to the highest resolution shell.

[b] Rmerge = ΣhΣj|Ihj−<Ih>|/ΣhΣjIhj, where Ihj is the intensity of observation j of reflection h.

[c] As defined by (Karplus and Diederichs, 2012)

[d] R = Σh|Fo|−|Fc|/Σh|Fo| for all reflections, where Fo and Fc are observed and calculated structure factors, respectively. Rfree is calculated analogously for the test reflections, randomly selected and excluded from the refinement.

[e] As defined by Molprobity (Davis et al., 2004)

Table 2.

Structural homologs of CdiA-CT•CdiI^{Kp342} and CdiA-CT•CdiI^{EC3006}, See also Figure S5.

Query protein	Homolog (organism)	PDB ID[a]	Z-score	rmsd[b] (Å)	lali/nres[c]	% identity
CdiI^{Kp342} (B)	β-galactosidase (*Escherichia coli*)	5TTG (A)	5.6	3.6	85/1015	9
	galactose mutarotase (*Lactococcus lactis*)	1NSS (B)	5.2	4.3	89/346	9
	lysyl oxidase (*Komagataella pastoris*)	1N9E (A)	5.2	4.4	71/735	8
	copper amine oxidase (*Arthrobacter globiformis*)	5ZPE (B)	5.1	4.3	80/620	6
CdiA-CT^{Kp342} (A)	colicin D (*E. coli*)	1V74 (A)	5.5	3.5	81/107	9
	colicin D (*E. coli*)	1TFO (A)	5.5	3.4	79/103	9
	BrnT (*B. abortus*)	3U97 (A)	5.1	2.5	65/77	9
	HigB2 (*V. cholerae*)	5JA8 (C)	5.0	3.4	73/108	10
	colicin D (*E. coli*)	1TFK (A)	4.5	3.5	69/94	7
	CdiA-CT^{NC101} (*E. coli*)	5I4Q (A)	4.5	3.1	70/88	7
CdiI^{EC3006} (C)	AP-1 complex subunit β1 (*Homo sapiens*)	4P6Z (B)	9.1	3.4	133/570	8
	Puf5p (*Saccharomyces cerevisiae*)	5BZV (A)	8.9	3.5	133/364	9
	importin β1 (*Saccharomyces cerevisiae*)	2BKU (B)	8.7	3.5	143/857	9
	glomulin (*Homo sapiens*)	4F52 (F)	8.6	3.5	143/512	8
	importin-4 (*Homo sapiens*)	5×BK (D)	8.6	3.7	137/369	8
	transportin-1 (*Homo sapiens*)	4JLQ (A)	8.6	3.5	132/840	8
CdiA-Ct^{EC3006} (A)	ParE (*Mesorhizobium opportunistum*)	5CEG (B)	4.6	3.9	74/103	5
	ParE2 (*E. coli* str. SS52)	5CW7 (P)	4.4	3.3	67/95	4
	ParE (*Caulobacter vibrioides* CB15)	3KXE (B)	4.1	3.5	71/94	6

[a] Homologous chains are given in parentheses.

[b] root-mean-square deviation.

[c] length of alignment (lali)/total number of residues (nres)

KEY RESOURCES TABLE

REAGENT or RESOURCE	SOURCE	IDENTIFIER
Antibodies		
rabbit polyclonal antisera to the CdiA^{EC393} TPS transport domain (residues Val33 – Gly285)	(Ruhe et al., 2015)	N/A
IRDye® 800CW goat anti-rabbit IgG	LI-COR	Cat# P/N 925-32211
Bacterial and Virus Strains		
E. coli B sub-strain BL21 (DE3)	Agilent	Cat# 200131
E. coli K-12 sub-strain MG1655	*E. coli* Genetic Stock Center	Strain #7740
E. coli K-12 sub-strain EPI100	Epicentre/Lucigen	Cat# EC10010
E. coli K-12 sub-strain X90		N/A
E. coli: CH2016: X90 (DE3) Δ*rna* Δ*slyD::kan*	(Garza-Sanchez et al., 2011)	N/A
E. coli: CH7157: X90 Δ*clpX* Δ*clpA::kan*	(Nikolakakis et al., 2012)	N/A
E. coli: CH8251: MC4100 *rif*^{R}	(Willett et al., 2015)	N/A
E. coli: CH12738: MG1655 *ara::spc*	(Jones et al., 2017)	N/A
E. coli: CH12739: MG1655 *ara::spc tsf(A202E)*	(Jones et al., 2017)	N/A
E. coli: CH12740: MG1655 *ara::spc tsf*(Δ*coil)*	(Jones et al., 2017)	N/A
E. coli: CH15087: EPI100 *mup*^{R}	This paper	N/A
E. coliI: DY378: W3110 l*cI857* Δ*(cro-bioA)*	(Thomason et al., 2007)	N/A
Biological Samples		
Chemicals, Peptides, and Recombinant Proteins		
Critical Commercial Assays		
The Protein Complex Suite	Qiagen	
Deposited Data		
Structure data and refinement statistics for CdiA-CT•CdiI^{Kp342} complex	This paper	PDB: 6CP9
Structure data and refinement statistics for CdiA-CT•CdiI^{EC3006} complex	This paper	PDB: 6CP8
Experimental Models: Cell Lines		

REAGENT or RESOURCE	SOURCE	IDENTIFIER
Experimental Models: Organisms/Strains		
Oligonucleotides		
Complete list of oligonucleotides and PCR primers	This paper	see Table S3
Recombinant DNA		
pET21b	Novagen	Cat# 69741-3
pTrc99A	Amersham	N/A
pCH978	This paper	N/A
pCH6283	Genscript	N/A
pCH6289	Genscript	N/A
pCH7171	(Johnson et al., 2016)	N/A
pCH8001	(Beck et al., 2014)	N/A
pCH10163	(Morse et al., 2012)	N/A
pCH11483	(Willett et al., 2015)	N/A
pCH11526	(Willett et al., 2015)	N/A
pCH11948	This paper	N/A
pCH12158	This paper	N/A
pCH12602	(Jones et al., 2017)	N/A
pCH12603	(Jones et al., 2017)	N/A
pCH12802	This paper	N/A
pCH12861	This paper	N/A
pCH12865	This paper	N/A
pCH12898	This paper	N/A
pCH13677	(Willett et al., 2015)	N/A
pCH13813	This paper	N/A
pCH13887	This paper	N/A
pCH13888	This paper	N/A
pCH13890	This paper	N/A
pCH13892	This paper	N/A
pCH13893	This paper	N/A
pCH13894	This paper	N/A
pCH13895	This paper	N/A
pCH13896	This paper	N/A

REAGENT or RESOURCE	SOURCE	IDENTIFIER
pCH14200	This paper	N/A
pCH14201	This paper	N/A
pCH14278	This paper	N/A
pCH14279	This paper	N/A
pCH14280	This paper	N/A
pCH14281	This paper	N/A
pCH14282	This paper	N/A
pCH14301	This paper	N/A
pCH14912	This paper	N/A
pCH14913	This paper	N/A
pCH14982	This paper	N/A
pMCSG63	(Eschenfeldt et al., 2009)	N/A
pMCSG63-APC111476	This paper	N/A
pMCSG63-APC200209	This paper	N/A
pMCSG63-APC200215	This paper	N/A
Software and Algorithms		
Chimera	(Pettersen et al., 2004)	https://www.cgl.ucsf.edu/chimera/
PHENIX	(Adams et al., 2010)	https://www.phenix-online.org/
Coot	(Emsley and Cowtan, 2004)	https://www2.mrc-lmb.cam.ac.uk/personal/pemsley/coot/
HKL-3000	(Minor et al., 2006)	http://www.hkl-xray.com/hkl-3000
Other		